AD NUMBER

AD476809

LIMITATION CHANGES

TO:

Approved for public release; distribution is unlimited. Document partially illegible.

FROM:

**Distribution authorized to U.S. Gov't. agencies and their contractors;
Administrative/Operational Use; DEC 1965. Other requests shall be referred to Army Missile Command, Redstone Arsenal, AL. Document partially illegible.**

AUTHORITY

usamc ltr 23 aug 1971

SEMIANNUAL REPORT OF RESEARCH IN TURBULENT WAKES

Sponsored by
U.S. Army Missile Command
under
Contract DA-01-021 AMC-11990 (Z)
and
ARPA Order No. 133, Amendment 9

SEMIANNUAL TECHNICAL SUMMARY REPORT

for the period
1 July 1965 to 31 December 1965

BSR 1236

This work has been accomplished as a part of PROJECT DEFENDER for the ADVANCED RESEARCH PROJECTS AGENCY (ARPA)

Project Code No. 5740

THE BENDIX CORPORATION
Bendix Systems Division
Ann Arbor, Michigan

FOREWORD

This semiannual progress report on Research in Turbulent Wakes by The Bendix Corporation, Bendix Systems Division, is submitted in keeping with Contract DA 01-021-AMC-11990 (Z). This research is sponsored by the U.S. Army Missile Command and the Advanced Research Projects Agency as part of Project DEFENDER, and covers cooperative research being carried out by Bendix Systems Division and the Canadian Armament Research and Development Establishment (CARDE). This report covers the initial period of the contract from 1 July 1965 through 31 December 1965, and includes a discussion of technical findings and a narrative description of program progress.

TABLE OF CONTENTS

ILLUSTRATIONS

SECTION 1

INTRODUCTION

The joint Bendix-CARDE Program has the following objectives:

1. To develop a hypervelocity ballistic range facility capable of reliably firing cones of 2-in. base diameter at velocities of 16,000 ft/sec.

2. To develop instrumentation to measure statistical properties of turbulence.

3. To obtain and analyze data using the instruments developed.

This report reflects progress toward these goals achieved during the second half-year.

SECTION 2

CARDE PROGRAM

2.1 LOCALIZED WAKE MEASUREMENTS STUDIES

2.1.1 Measurements of Mass Density Fluctuations

2.1.1.1 Electron Beam Probe

The prototype electron beam generator described in the June 1965 Progress Report has been used on Range 3 to obtain preliminary measurements. The beam generator has been installed on a new test section in Range 3. With this arrangement, the range axis is only 7.5 inches from the beam entrance in the range. The usable beam length with a 0.6 torr range pressure is approximately six inches.

Two difficulties were encountered and solved before the measurements were obtained. The first problem was the large AC fluctuations superimposed on the beam current. These fluctuations were similar to a ripple and were as large as 50% of the total beam current. It was found that these variations were due to the ripple on the accelerating high voltage supply. A ripple filter was built to reduce the high voltage ripple from 5% to 0.5% peak-to-peak. With the rippler filter and magnetic shielding around the TV electron gun, the beam current ripple was reduced below the noise level of the light detectors.

The second difficulty came from stray radiation seen by the three light detectors. The stray radiation was produced by the projectile impact flash reflected from the test section walls. This radiation was eliminated by improving the light baffles in both the light collector and test section, and by impacting the projectile outside the range tank by firing through a rubber diaphragm.

Preliminary measurements of density behind a hypervelocity projectile have been obtained. Twelve firings of one inch diameter aluminum spheres at a velocity between 10,000 fps to 12,000 fps at a range pressure of 0.6 torr have been recorded on three detectors. A typical detector record is shown in Fig. 2-1. The density ratio behind a one inch sphere for three radial positions is given in Fig 2-2. We see the radial density ratio measured at various positions behind the projectile in Fig 2-3. The results from several firings are used to construct this figure.

A more powerful electron beam generator has been purchased from Ontario Research Foundation. This generator can produce a 100 KV one milliamp beam of 1.5 mm diameter. A comparison of the two electron beam generators is given in Fig 2-4. The 100 KV electron beam generator will be in operation on Range 5 in January 1966.

2.1.1.2 Density Measurement by Rayleigh Scattering of Ruby Laser Radiation

Calculations show that the ratio of the Rayleigh scattered intensities (I_s) to incident intensities (I_o) is proportional to the mass density of air for $T < 3000^{\circ}K$ and $\rho / \rho_o \lesssim 10^{-3}$. It is therefore possible to follow mass density fluctuations in a turbulent air wake by following fluctuations in the ratio, I_s/I_o. Since this ratio is very small, being only 10^{-13} under even optimum experimental conditions, it is necessary to use a ruby laser as the light source. A Maser Optics 3100 Ruby Laser, which is rated at a nominal maximum output of 125 joules, is being used in the burst mode of operation with liquid nitrogen cooling. Under maximum operating conditions, a pulse is obtained with a peak power of approximately 100 KW and a duration of 1.7 milliseconds. The scattered radiation will be gathered by a lens situated at a distance of three feet from the center of the range and oriented 45° to the incident beam. An RCA 7265 photomultiplier will be used to monitor the scattered radiation. These components are now under construction and efforts are being made to install them on Range 5 by the end of December or the beginning of January 1966.

2.1.2 Measurement of Electron Density

The conductivity probe is now in routine operation. Its overall length has been reduced. The probe electronics, previously a single unit located near the probe inside the range, have been split into an epoxy-encased preamplifier mounted rigidly on the probe itself and a line driving amplifier mounted external to the range. The smaller probe and "potted" preamplifier combination is not sensitive to vibration and shock so that microphony is no longer a problem.

Many rounds have been observed in Range 3 using equipment similar to the present version. Experience has shown that signals which are useful for analysis are obtained only when the projectile (sphere) passes within one body diameter of the probe. Of recent rounds in Range 3, many have met this requirement.

At the moment two special probes are being readied in Range 3. The first is a stagnation probe. The data from this is to be compared with ordinary probe data to determine whether stagnation by a probe will seriously influence the measurements. A probe has been constructed with two separate

electron collectors fixed about 1/4 inch apart in a single molded surface. It is possible that this double collector probe can be used to check certain statistical assumptions and to make wake velocity measurements.

A few rounds have been observed in Range 5, but little data has been obtained so far. The data obtained has corresponded to that from Range 3. In the future, most work will be done on Range 5 except for minor study on Range 3. All information so far has come from spheres and no wake has ever been detected behind a cone. It may be necessary to enhance ionization behind cones. In the case of spheres, the duration of observation is less than desired and it may also be necessary here to lengthen the recording time by ion augmentation. These problems are now being studied.

2.1.3 Measurement of Axial Wake Velocity Distribution

Significant progress has been made on this problem during the past six months. In the previous semi-annual report, data from the first exploratory round was given. The behavior of the overall system was nearly unknown at that time. Presently 30 rounds have been fired on Range 2. The geometrical symmetry of the electrodes were verified by an electrolytic bath in such a way that the spark jumped directly from one electrode to the other. A curved spark is nearly always associated with a nonsymmetrical electrostatic field between the electrodes. A block circuit diagram is given in Fig. 2-5. A few of the rounds were analyzed and it was soon found that it would be necessary to have a complete stereo-readout system in order to determine where the spark passed in the wake of the projectile. This is necessary when the round does not pass directly between the electrodes. A stereo system was designed, and with this system it is possible to determine within a millimeter the position of each spark in three dimensions.

A typical seven pulse spark sequence photographed at 30° aspect angle, Fig. 2-6. As far as could be ascertained from the views at 30° and 90° the sparks were flat and passed directly across the wake. The variation in velocity is given in Fig. 2-7. Here the near wake velocity is 1200 feet per second in the center of the wake.

This method has considerable potential in the determination of wake velocity. Modifications are presently under way to permit an electrode spacing of ten inches instead of the present five inches. The present spacing is adequate for one inch spheres and cones, but a ten inch separation is required for the 2.7 inch spheres and two inch base diameter cones being fired on Range 5.

2.1.4 Hot Wire Anemometer

Since the last semi-annual report, some ten to fifteen rounds have been observed with a constant current hot wire anemometer system. Different

probe configurations have been used with all probes at different radial distances from the flight axis or at the same radial distance from the flight axis but at various axial distances.

Sensors have been fabricated from 0.0002 inch diameter platinum wire and 0.0001 inch diameter tungsten wire. Their temperatures were adjusted to 250°C - 300°C above the ambient static temperature.

Experimental results have been obtained from cones fired on Ranges 3 and 5. Velocities have varied between 14,000 and 16,000 feet per second. Ambient pressures were 130 mm of Hg in an air atmosphere.

A phenomenological study of the hot wire traces has shown that hot wires respond mainly to changes in mean flow quantities produced by the shock waves from the projectile. These include both the bow shock envelope and the reflected shocks. No velocity, temperature or density fluctuations which could be attributed to turbulence have been measured up to the present time.

2.1.5 Data Recording, Conversion and Analysis

The previous semi-annual report described the data processing procedure. In brief, signals arising from various probes and detectors in the range are fed into oscilloscopes and then recorded by Polaroid or Fastax cameras. The resulting film traces are converted to digitized records by means of a flying spot scanning device. The digital records are processed by a computer to produce estimates of autocorrelation functions and power spectra.

2.1.5.1 Recording System

So far the recording systems appear to be adequate for the bandwidths of the signals being recorded.

2.1.5.2 Analog to Digital Conversion

Generally, the resulting of the flying-spot-scanner apparatus are extremely reproducible. Some erroneous output results have been noted, and by comparing the input and output results, the effect was traced to a lack of sufficient contrast on inverted film records. This deficiency should be easy to remedy.

2.1.5.3 Autocorrelation and Spectral Analysis Program

The machine program for autocorrelation function calculation and spectral analysis has been modified so that it corresponds to the method prescribed by Blackman and Tukey (Reference 1). The new program has been

verified by hand calculation and by analysis of a known noise source, and is now ready for analysis of probe time records.

2.1.5.4 Statistical Precision

The time histories of probe signals from a ballistic range are extremely short; in addition, it is necessary to further subdivide these records because of the variation of the wake velocity with distance behind a projectile. A preliminary analysis of the likely precision of anticipated power spectral estimates have been undertaken according to the procedure of Blackman and Tukey.

2.2 HYPERVELOCITY LABORATORY TECHNIQUES

2.2.1 Launcher Ballistics

The development of a computer program for the solution of a modified Constant Base Pressure Launcher has been completed by Computing Devices of Canada (CDC). Information pertaining to a heavy piston computer case fired at CARDE was sent to CDC for correlation with microwave and piezo gauge information acquired from the shot. Results of the calculation are expected shortly.

A comparison of Ballistic Research Laboratory (B.R.L.) computer results and CARDE experimental results for a number of shots made during the period showed good agreement. This was reported at the Aeroballistic Range Association meeting and is the subject of a forthcoming report (Reference 2.).

A diaphragm development program has indicated the superiority of having the initial throat section square rather than round. Release pressure was increased by 50% and there was no sign of tearing of the corners of the petals.

Propellant chamber design for the 10/4 gun is completed insofar as the dimensions required for mechanical design are concerned. Computer results from the CDC program will be required to improve performance.

Three papers (References 2-4) were presented at the Aeroballistic Range Association meeting and one Technical Memorandum is in the process of publication.

2.2.2 Launch Techniques

One inch diameter bimetal cones have been successfully launched with 70% reliability from a three piece petalling sabot at 16,000 feet per second on Range 3 at a pressure of 130 mmHg. One inch diameter metallic

and plastic spheres have also been successfully launched with 90% reliability from two piece petalling sabots at velocities ranging from 11,000 to 18,500 feet per second and range pressures from 30 microns to 76 mmHg.

For the 10-4 light gas gun on Range 5, results showed good in-flight stability for the two inch diameter 20° cones at 15,000 feet per second and 140 mmHg, but some problems were encountered with sabot petal breakage during the sabot discard. Further study is presently underway to improve the stress analysis. The problem may be due to a barrel misalignment, bore condition, or transient dynamic loading resulting from vibration.

Considerable theoretical work was done on sabot design with special emphasis on the loading of the sabot during the aerodynamic discarding phase.

Spheres of .217 inch and 2 inch diameters have been successfully launched in Range 5 at 16,000 feet per second and 130 mmHg, but some problems were encountered in spalling or frontal damage to the spheres, probably caused by shock wave propagation through the sabot and sphere materials. Also this damage could possibly have been caused by impacting on the microwave reflectors at the muzzle or the mylar diaphragm between the dump tank and range. In order to understand the damage due to shock wave propagation, a theoretical study of shock patterns in spheres was carried out. This study indicated that hollow spheres are less subject to front face spalling.

A study of cones indicated that failure of "Kevimet" tipped cones was likely to occur as had been experienced in the testing. An attempt was made to apply the theory to a steel tipped cone, and although the theory indicated that the model should have failed, it did not. Further work is required on this problem.

Interest has also been expressed by the program originators concerning the feasibility of studying mass transfer into the boundary layer of a cone from its pressurized hollow interior. A design study is presently underway. Contact has been established with different agencies that have done similar studies as well as manufacturers of transpiring materials.

Figure 2-8 present five x-ray photos of sabot discard for spheres and cones. It is by means of this technique that insight can be gained into the complex opening mechanisms during sabot discard.

The quarter wave length method for control of angle of attack has been adapted to Range 5. Briefly, this principle makes use of a dump tank configuration that permits the cone to enter the evacuated tank at its maximum angle of attack and hence its minimum angular rate. Experiments on Range 3

showed however, that the motion of angle of attack of the cones is not planar, but rather epicyclic. Thus, there are no points for which angular velocities are zero. It is possible to achieve the lowest angle of attack variations by ushering the projectile into the dump tank at a point where the angular velocity is a minimum, i. e. at the ends of the major axis of the angle of attack ellipse.

Range 3 results indicate this point of minimum angular velocity is predictable, and results were scaled to Range 5 giving a distance for X_{umax} of about 85 feet. Recent Range 5 tests have indicated that X_{umax} distance has an average value of 90 feet where u is total angle of attack.

It appears, therefore, that some angle of attack control is possible, and although oscillations will not be totally elminated, they can be reduced to minimum values.

2.2.3 Reliability

Reliability has been stressed over the past several months as this is one area where reducing the number of shots necessary for a data point can substantially reduce the time element and cost of running the program. Figures 2-9 and 2-10 graphically present cone launch reliability and operations reliability for the period 1 July 65 through 15 October 1965.

2.2.4 Instrumentation

2.2.4.1 Precision Photo Attitude Measurements

The development of a precision stereo photo attitude system has continued during the past six months on both Ranges 3 and 5. All of these stations are based on the single film, double x-ray head principle. Stations on both ranges were designed with three feet separation between the x-ray sources.

The six Range 3 installations employ drill tables with simple rack and pinion height adjustments which permit easy movement of the x-ray heads within one mil in any direction. The included angle between the two x-ray heads is 55°.

Range 3 stations have been in operation for the past four months and are giving precise results. Measurement precision is at least $\pm$ 0.05 inches.

Five stations are installed and working on Range 5. These stations use a different design, having only one box to mount both x-ray pulsers. The box is supported by a central adjustable axle. The included angle between heads is 30° in this case, compared to 55° on Range 3. The precision is not as high as on Range 3 presently due to the different geometry. However, it is expected

that with an accurate survey, Range 5 measurements will be made within 0.02 inches. Six more stations have been purchased for Range 5, and will be installed within the next four months.

An analog data reader has been designed based on the superposition principle, and will be under construction sometime during the three months.

2.2.4.2 Gun Barrel Velocity Measurement Radar

A X-band doppler radar has been used to determine the projectile velocity and acceleration within the Range 5, four inch gun barrel. It has been determined that the velocity of the piston in the pump tube can also be measured. This measurement is possible because the sabot is constructed of plastic which is transparent to microwaves. The dopper return signal was increased by placing aluminum foil on the front face of the piston.

On Range 3, a K-band doppler system has been built and will soon be used on a firing. X-band was chosen because the wave length diameter ratio of the 1 1/2 inch barrel at X-band could subject the transmission to high attenuation in the gun barrle. The wave length diameter ratio at X-band becomes a similar to that of the four inch barrel at X-band.

2.2.4.3 Strain and Vibration Measurements on Light Gas Guns

Strains have been monitored both dynamically and statically on the Range 3 and Range 5 guns during the past six months. Proofing has been conducted on the new high pressure section for the 4 - 1 1/2 inch gun, and it was found that it was possible to increase the velocity of this gun to 18,600 feet per second without any appreciable residual strains. In addition, monitoring was conducted on the Range 5 gun when studies were conducted on heavier pistons.

The measurement of vibration has continued and has been conducted both by using strain gauges and vibration transducers. Measurements will soon include the use of an absolute displacement transducer which functions on a magnetic principle without any contact with the moving surface. These transducers have a 100 kilocycle response.

2.2.4.4 Photo Attitude Triggers

The triggers described in the last semi-annual report are working quite well and no unforeseen problems have arisen. At present these triggers cover a horizontal displacement of approximately fourteen inches. Further development work will be necessary before a full forty-eight inch trigger is available for use on Range 5. This is the ultimate photo attitude capability of the Range 5 stereo flash x-ray system.

2.2.4.5 Range Firing Control Center

During the past six months the Range 5 control center has been modified to include the controls for the Range 3 gun. Ranges 3 and 5 are now being fired from the same control center. The gas loading panels, vacuum panels and firing panels are separate for each range. The flight instrumentation, velocity and pressure measuring systems are common to both ranges. A new jack field is presently being installed and should be ready within the next four or five months. This will provide a rapid change-over of cables from Range 3 to Range 5 using the common instrumentation console.

ELECTRON BEAM MEASUREMENT OF DENSITY VARIATION ALONG WAKE.

POSITION. 0.8 INCH OFF AXIS.

PROJECTILE: ONE INCH DIA. AL SPHERE
VELOCITY: 12,140 F.P.S.
RANGE PRESSURE: 580μ HG.

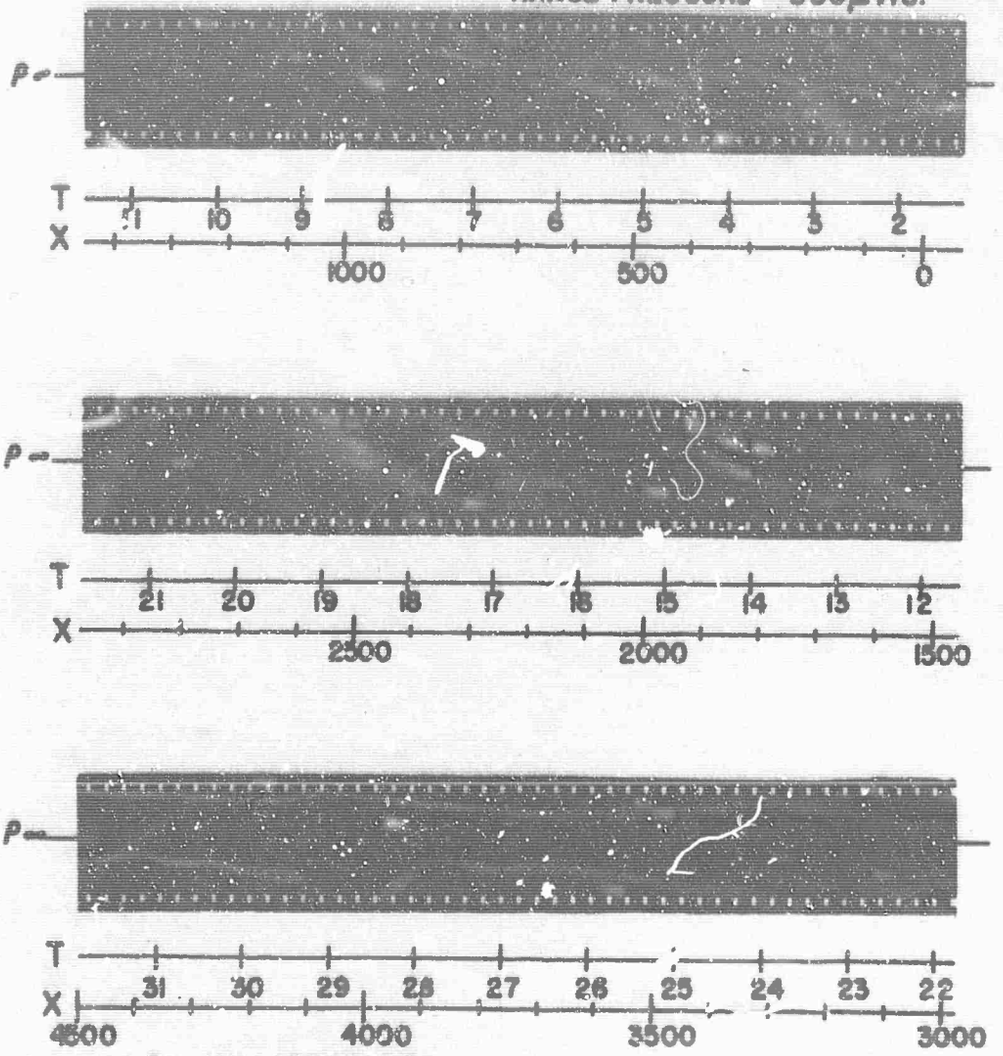

T = MILLISECONDS.
X = BODY DIAMETER.

FIGURE 2-1

MEASURED RELATIVE WAKE DENSITY AT THREE RADIAL POSITIONS

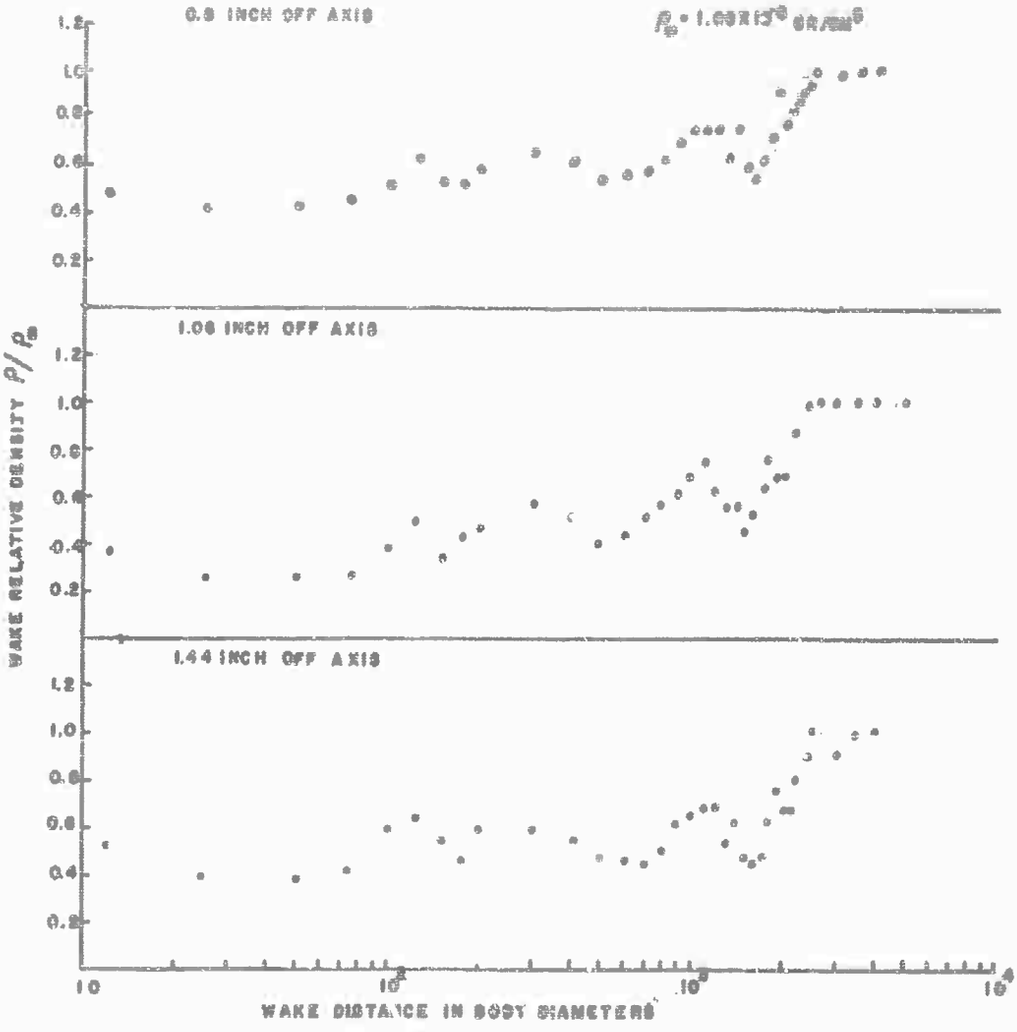

FIGURE 2-2

VARIATION OF RADIAL DENSITY RATIO

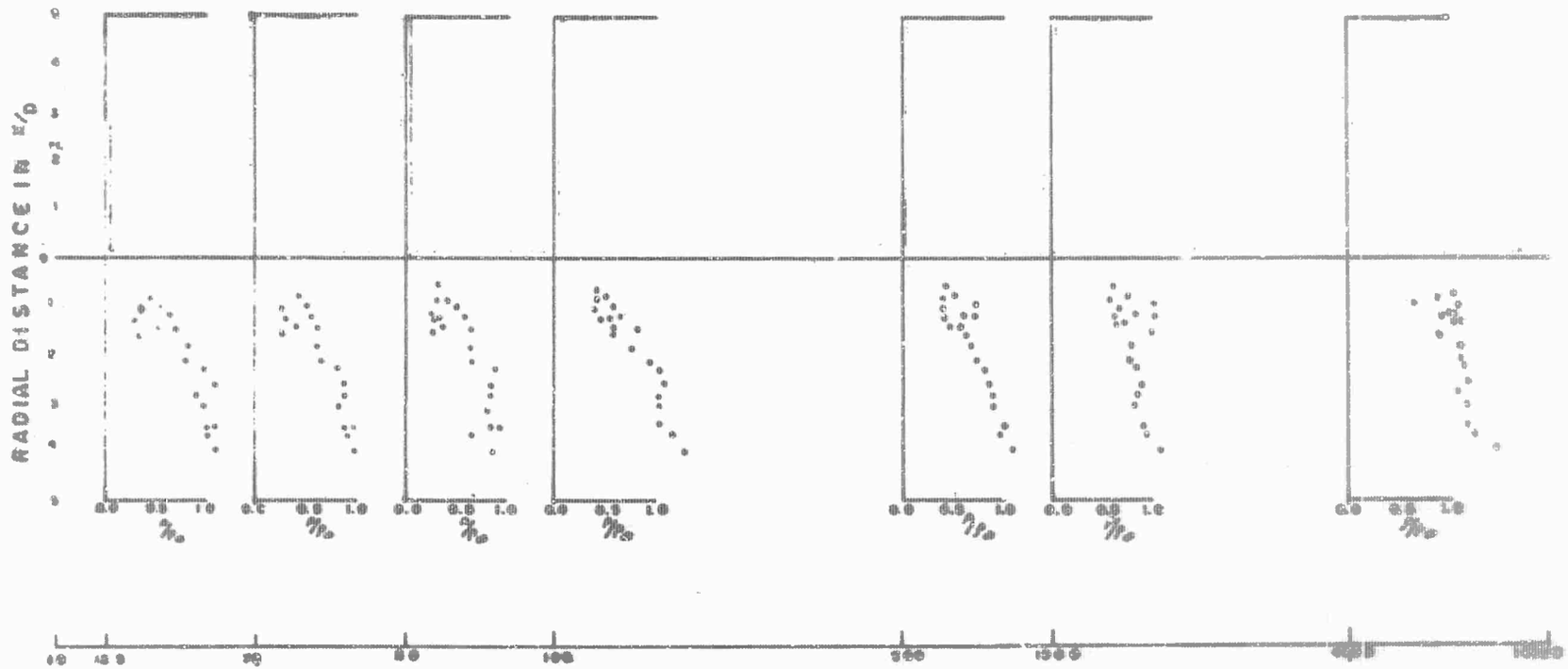

FIGURE 2-3

	V KV	I MA	P TORR	ρ MG/CM^3	S μA	$\frac{dE}{dx}$ KeV/MG/CM^2	R MG/CM^2	Rs FOR STOPPING CM	0.01 Rs CM	
CARDE RANGE 3	23	0.2	0.6	9.6×10^{-4}	42	11	1.25	1.33×10	13.3	
ORF RANGE 5	100	1.0	10.0	1.61×10^{-2}	225	3.5	14.5	9×10^{2}	9.0	
ORF RANGE 5	100	1.0	0.6	9.6×10^{-4}	14	3.5	14.5	1.5×10^{4}	150	
ORF	40	1.0	0.6	9.6×10^{-4}	2.8	7	3.0	3.12×10^{3}	30	
ORF	100	1.0	3.0	4.83×10^{-3}	6.8	3.5	14.5	3×10^{3}	30	

CAPABILITIES OF ELECTRON BEAM GENERATORS.

FIGURE 2-4

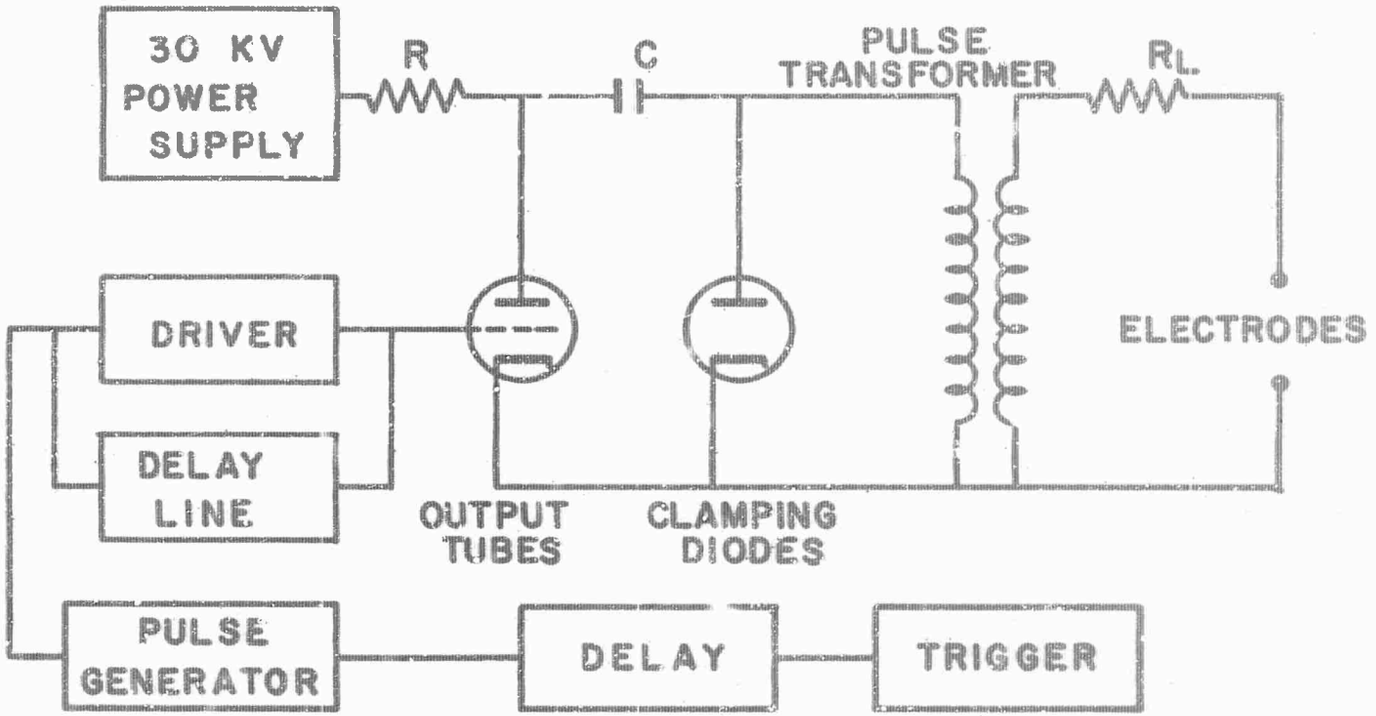
30 KV
POWER
SUPPLY
R
C
PULSE
TRANSFORMER
RL
DRIVER
DELAY
LINE
OUTPUT
TUBES
CLAMPING
DIODES
ELECTRODES
PULSE
GENERATOR
DELAY
TRIGGER

FIGURE 2-5

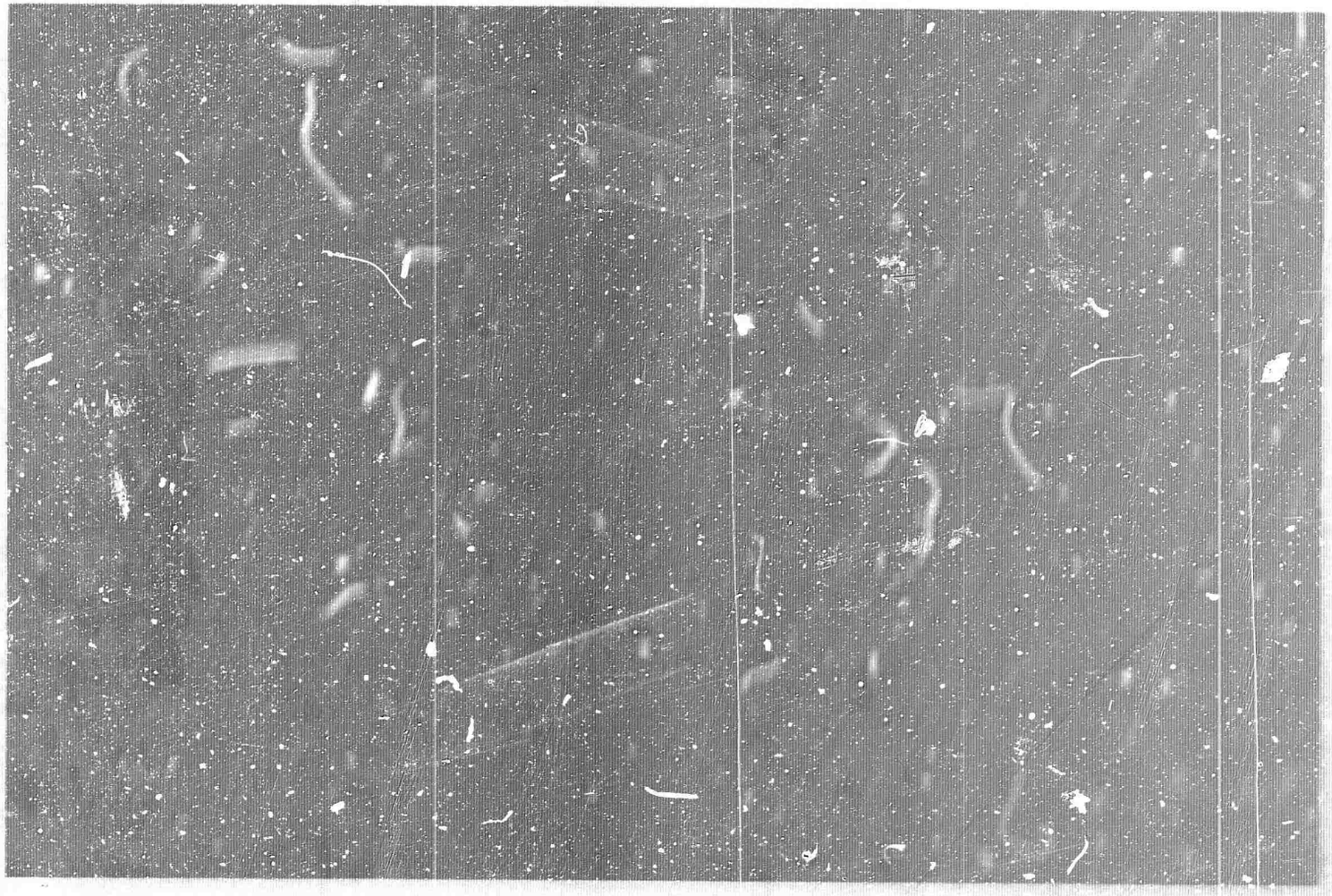

Typical Spark Sequence
FIGURE 2-6

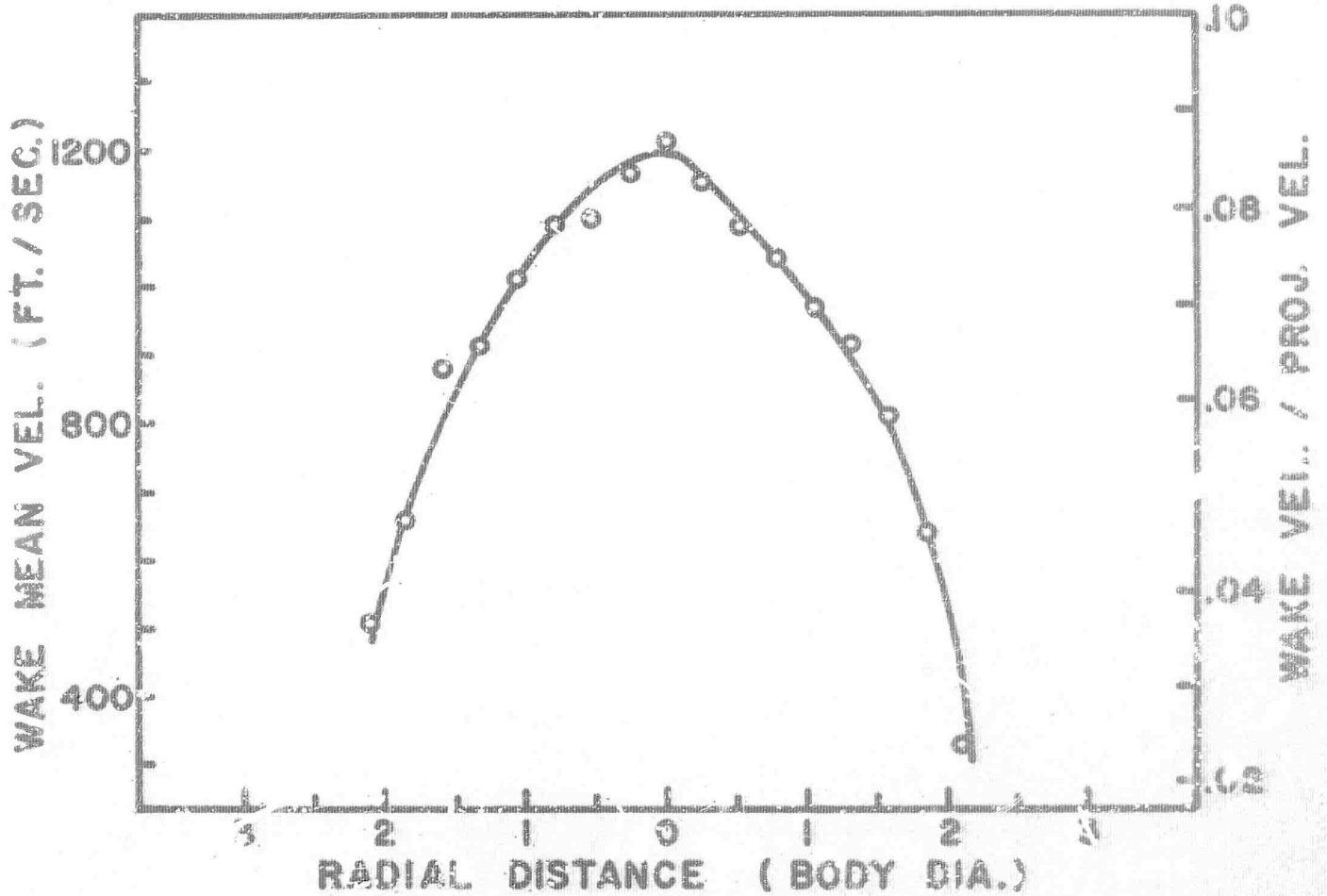

FIGURE 2-7

MEAN WAKE VELOCITY vs RADIAL DISTANCE

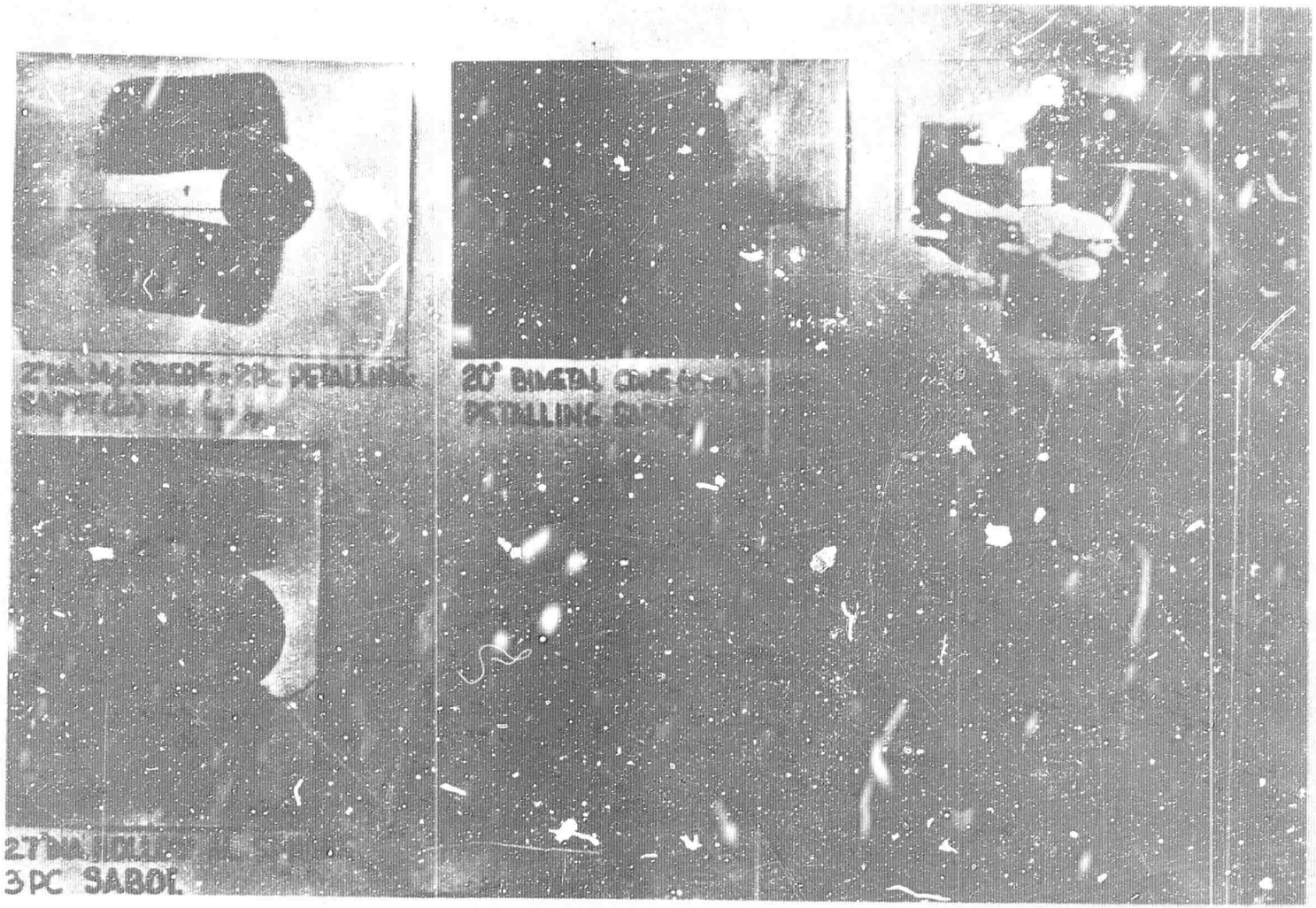

FIGURE 2.8
X-RAY PHOTOS OF SABOT DISCARD FOR SPHERES AND CONES

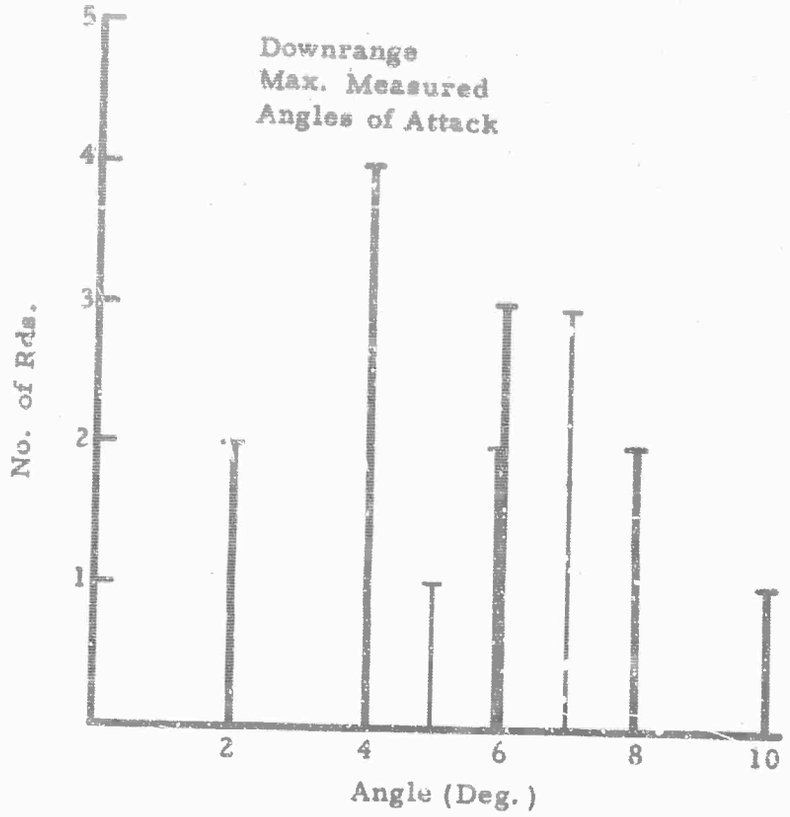

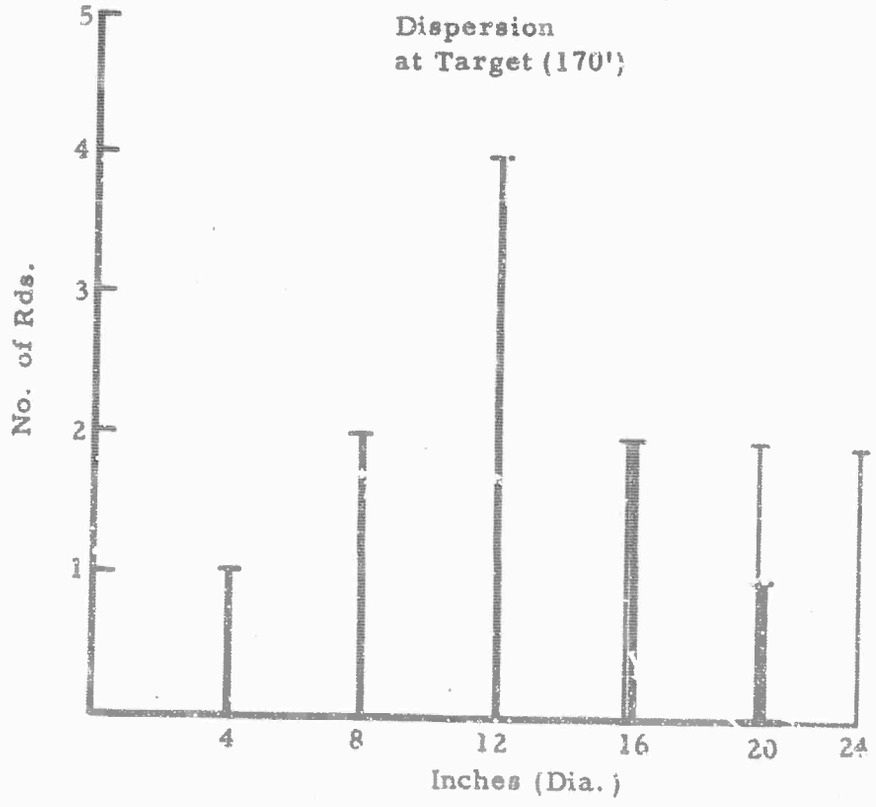

FIGURE 2.9

RANGES 3&5 CONE LAUNCH RELIABILITY (1 July - 15 October, 1965)

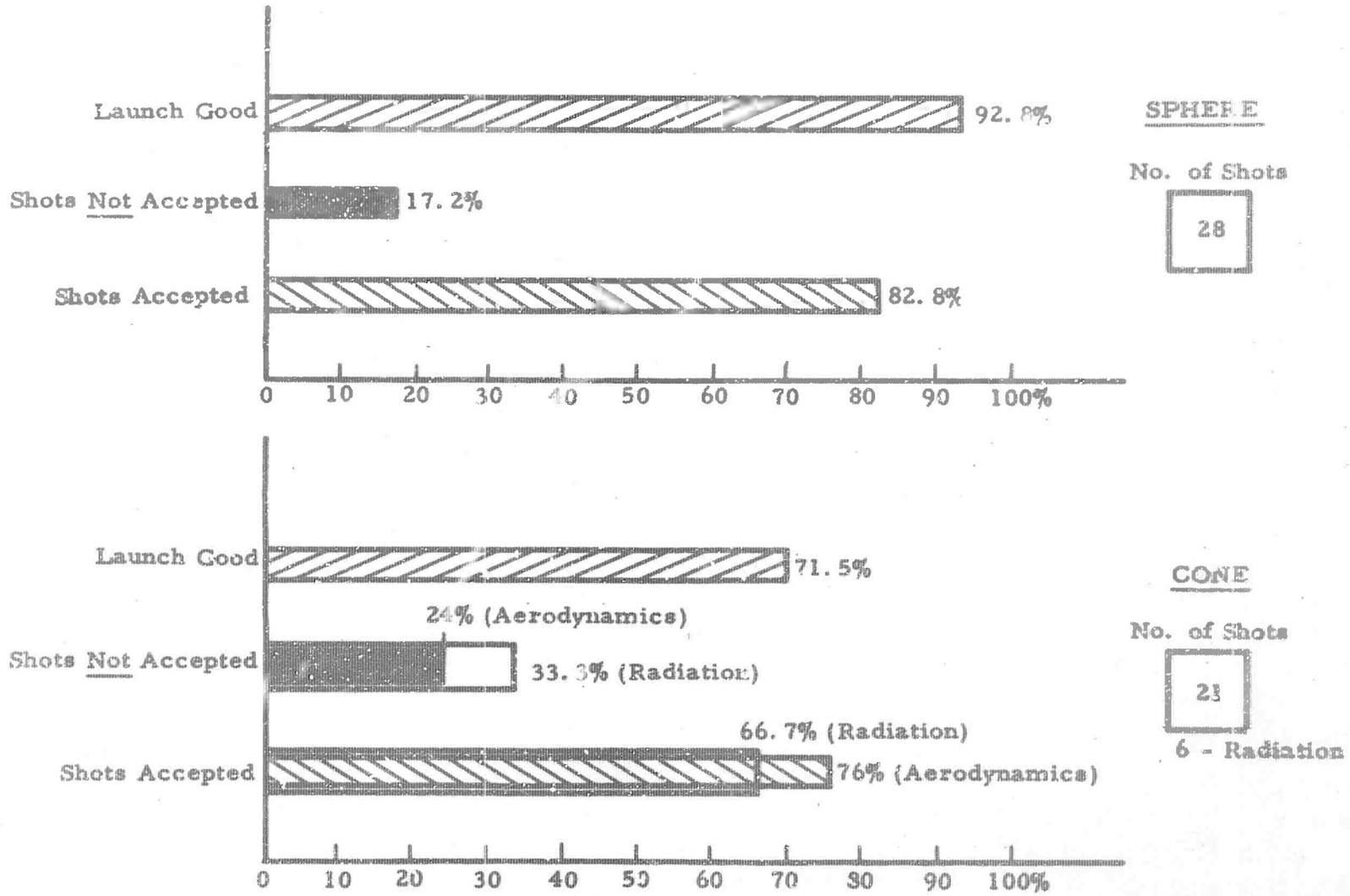

FIGURE 2.10

RANGE 3 OPERATIONS RELIABILITY

SECTION 3

BENDIX EFFORT

3.1 OPTICAL RADIATION CORRELATIONS AND SPECTRA

The photospectrocorrelator has evolved to the point where its uses as a turbulence diagnostic tool and calibration standard for other diagnostic devices render it indispensible to our plasma turbulence research program. Not only does it provide true RMS power spectra and spatiotemporal correlations of emitted light fluctuations but it provides the only means of obtaining:

a) the mean jet velocity

b) the true RMS value of a fluctuating quantity, i.e. emitted radiation.

Knowledge of the mean jet velocity is required in transforming spectra from frequency space to wave number space whereas the true RMS value of a fluctuating quantity is essential in the normalization of correlations taken within nonhomogeneous media. Although no rigorous mathematical connection has yet been established between the RMS values of simultaneously fluctuating disparate quantities, there is strong reason to believe that they behave similarly, e.g. RMS neutral and electron density fluctuations. In that event, the photospectrocorrelator will be useful in reducing scattered microwave signals to absolute cross-sections and in subtracting background variations from shadowgraph correlations.

3.1.1 Jet System Characteristics

The jet spectra obtained using narrow band filters exhibited well-defined peaks since they were not all obvious multiples of 60 cycles and in order to separate arc current modulation from actual turbulence, the spectrum of the arc power supply was measured using an induction coil. The arc current spectrum (Fig. 3.1) displays a delta-functional behavior whose largest contributions center around 360 cps and, surprisingly, 4000 cps. An interesting thing happens with regard to the latter spike when grids are inserted into the jet. Discussion is deferred until the next section.

Needed in the reduction of spatial correlation data is the RMS value of the light intensity fluctuation as a function of jet axial distance. This is shown, for the operating condition of the majority of the tests, in Fig. 3.2. Note the negative ten thirds power decay.

The light transmission characteristics of the optical system were obtained by traversing the lens diameter with the moveable photomultipler while viewing a flourescent tube aligned on the jet axis. The resulting curve, normalized to the value taken at a distance of 0.2 inches from the lens edge, is shown in Fig. 3.3.

The response of the temporal correlation subsystem to a truncated white noise spectrum is shown in Figure 3.4. Ideally, the response should be $(\sin\omega\tau/\omega\tau$ where ω is the cutoff frequency of the input spectrum. Inspection of Figure 3.4 discloses a slightly less than ideal behavior at low correlation values. This is due to residual electronic multiplier voltages and the finite roll-off rate of the 10 kc cutoff filter. The behavior for larger correlation values is quite accurate.

Analogously, the response of the spatial correlation subsystem was checked by placing a Ronchi grid over a fluorescent tube aligned along the jet axis. The output was a sequence of step functions modulated by the lens light transmission curve, Fig. 3.3.

Using the photocorrelator in its combined spatio temporal mode, an accurate value of the mean jet velocity may be obtained. The procedure is as follows:

1. The moveable phototube is displaced a known distance from the fixed phototube.

2. The upstream (fixed) phototube output is delayed and multiplied with the downstream phototube output. The product is displayed on a scope.

3. When the adjustable delay time does not correspond to the phototube separation divded by the jet velocity, the product contains numerous negative components. When the time delay is precisely equal to the above quotient, the finite persistence of the turbulence pattern reduces the number of negative product components to a minimum and the product display is nearly flat-bottomed. Incidentally, the product display is exactly flat-bottomed when the phototube separation and time delay are zero. Here, all the random components are in phase and the product cannot be negative.

The result of this operation for one operating condition with and without a grid inserted into the jet is shown in Fig. 3.5. Note that the velocity behind the grid is less than the corresponding velocity in a grid-free jet. This is due to standing shocks produced at the grid plane and energy

extracted by the grid. The microwave data bear this out; without a grid, the jet at this operating condition is overdense whereas with the grid, the jet is underdense.

Optically, the jet is visibly widened by the insertion of a grid but the specific luminosity is lessened. Measurements indicate that the two effects very nearly counterbalance each other with the net result that the integrated RMS value of the light fluctuation intensity is the same with or without a grid over an appreciable length of the jet.

3.1.2 Optical Power Spectra

Optical power spectra have been obtained for several axial positions and with grids inserted into the flow. Typical results are shown in Figures 3.6 to 3.8.

Figure 3.6 illustrates the two prominent power supply modulation peaks mentioned in Section 3.1.1. Note that, as a function of frequency, the decay exhibits an inverse second power behavior. These data will be replotted as a function of wave number with the aid of Figure 3.5 in order to facilitate comparison to microwave spectra.

Figure 3.7 illustrates the effect of inserting a tungsten biplanar grid of 1/2 inch mesh size into the flow of the previous figure. Note that the 4000 cycle per second peak has been demodulated. The decay rate follows an inverse seven-thirds power law.

The spectra of Fig. 3.8 illustrate the decay of total fluctuation power as a function of downstream distance. Note that viscosity destroys the power supply modulation as the flow progresses.

3.1.3 Optical Correlations

Figures 3.9 to 3.10 are typical of the correlations thus far obtained. They clearly illustrate the effect of grid insertion on three temporal correlations distinguished by their different input filters. The most significant effect of grid insertion is the damping of the correlation of high frequency components. Not immediately apparent from these curves is the significant result that spatial correlations are profoundly affected by grid insertion. This is due to the fact that the grid reduces the mean jet velocity so that the turbulence while still requiring the same integral time to become uncorrelated does so in a shorter distance (integral distance scale). It is probably safe to infer from this behavior that the random turbulence velocity (RMS) is much less than the mean jet velocity.

3.2 MICROWAVE SCATTERING FROM A TURBULENT PLASMA

The azimuthal bistatic microwave probe retains the same basic configuration as reported in the previous semi-annual report. There are, however, the following modifications:

1) Video diodes have been installed in the receiving channels.

2) The original klystron, operating at 55 kMc, wore out and has been replaced by a klystron of lower power output operating at 70 k Mc.

The first change allows the total energy of the scattered microwave signals to be monitored instead of only that doppler energy which lies above 4 kc. Its installation is not intended to replace the doppler analysis capability of the system but only to serve as an adjunct to it.

3.2.1 Overdense Scattering

The first series of doppler spectra obtained without the insertion of a grid into the flow display a behavior that is most easily explained by assuming that the scattering medium is overdense. Reasons for this belief will become apparent in the course of the discussion of the data. As with the optical data, the arc power and tank pressure have been held constant throughout.

Figure 3.11 illustrates the variation of the doppler spectrum as a function of downstream distance for a single scattering angle (120°). Note that the high frequency components decay as the flow progresses but that the total doppler energy within this particular solid scattering angle does not necessarily decrease*. (*On the contrary, it increases! More on that below.) The high frequency decay may be considered indicative of viscosity's diminution of the high random velocity small scale turbule population.

The total doppler return power as a function of azimuth and axial jet distance is shown in Fig. 3.12. Note the low value of forward scattering ($\theta = 0^{\circ}$). This is one indication that the plasma is overdense. The null in the return signal at $\theta = 90^{\circ}$ is also taken to be indicative of overdensity. At the time of these measurements, the latter phenomenon was unexpected and a number of possible explanations were advanced in addition to the one assuming overdensity. That it may have been due to jet aniostropy was ruled out when the return signal amplitude was found to be invariant with respect to jet nozzle rotation. That it may have been due to polarization effects was tenatively ruled out when the signal amplitude was measured with the receiving horn rotation 90° with respect to its original position. These

exclusions left the possibilities that the jet may be either overdense or that it may be some peculiarity characteristic of doppler scattering only.

The latter possiblity was investigated with the aid of the video diode installation. It was found that the total return power as measured by this means displayed a behavior similar to that of the total doppler return as a function of scattering angle (Figure 3.13).

The scattering data was integrated with respect to azimuth to obtain the total power scattered throughout all planar scattering angles. This appears in Figure 3.14. Note that the total scattered power increases with the first power of distance. The jet width obeys an identical law. This is another indication that the plasma is overdense. Note also that the total doppler power which depends upon velocity increases to a maximum and then decays, presumably just as the higher doppler velocities do.

With the installation of the new klystron at 70 GHz the azimuthal microwave scattering was again measured at one downstream position. Again the dip in the spectrum at 90^{o} appeared but was not as pronounced as with the lower frequency. Since the entire system was not calibrated, this spectrum (Figure 3.15) is only relative and cannot be compared absolutely to the calibrated 55 GHz measurements.

3.2.2 Underdense Scattering

The insertion of a grid (Section 3.1) into the jet has a profound effect upon the microwave spectrum. Because the grid extracts energy from the flow and provides a relatively cold third body to catalyze electron recombination, the plasma downstream of the grid is underdense. When the doppler spectra are integrated with respect to frequency to obtain the total doppler power and then plotted as a function of azimuth, the result is a spectrum in accordance with underdense scattering theory. Plotted versus scattering angle, θ, the spectral tail-off exhibits an inverse fourth power behavior (Figure 3.16). When the scattering angle is converted to turbulence wave number, $K = 2k \sin \theta/2$, $k = 14.6\ cm^{-1}$, the spectrum exhibits the behavior shown in Figure 3.17.

In the future, [illegible]tra will be refined by the inclusion of more experimental poi[illegible] [illegible]arsenass of the data at present is of course due to the length [illegible]eguide employed. Shorter sections will allow shorter increment[illegible]scattering angle to be taken.

Measurements of the temporal correlation of the microwave power are presently being initiated. Preliminary results indicate a behavior analogous to that of correlations obtained with the optical system.

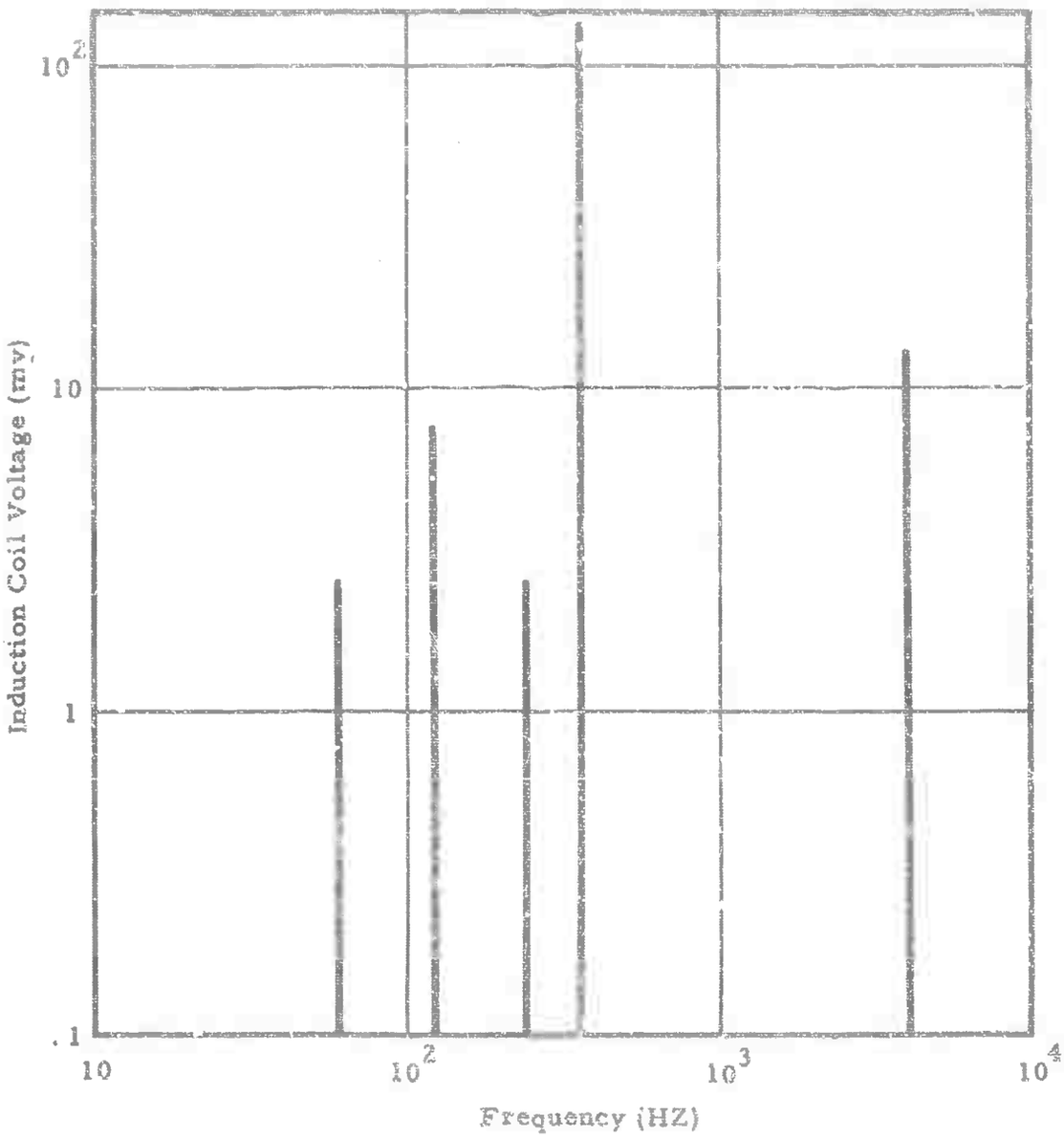

FIGURE 3.1
Spectrum of Arc Current

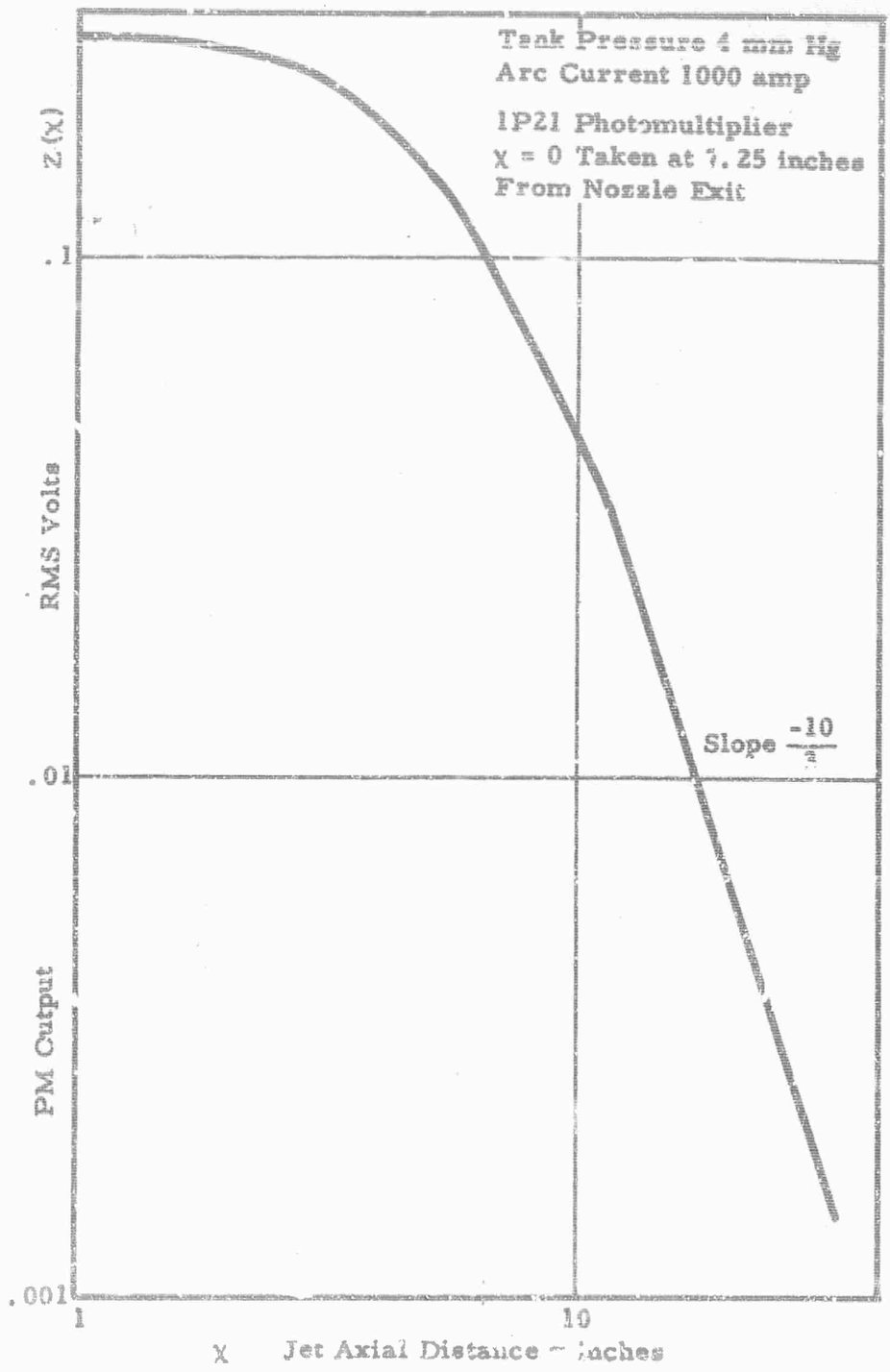

FIGURE 3.2
RMS LIGHT INTENSITY FLUCTUATION vs AXIAL DISTANCE

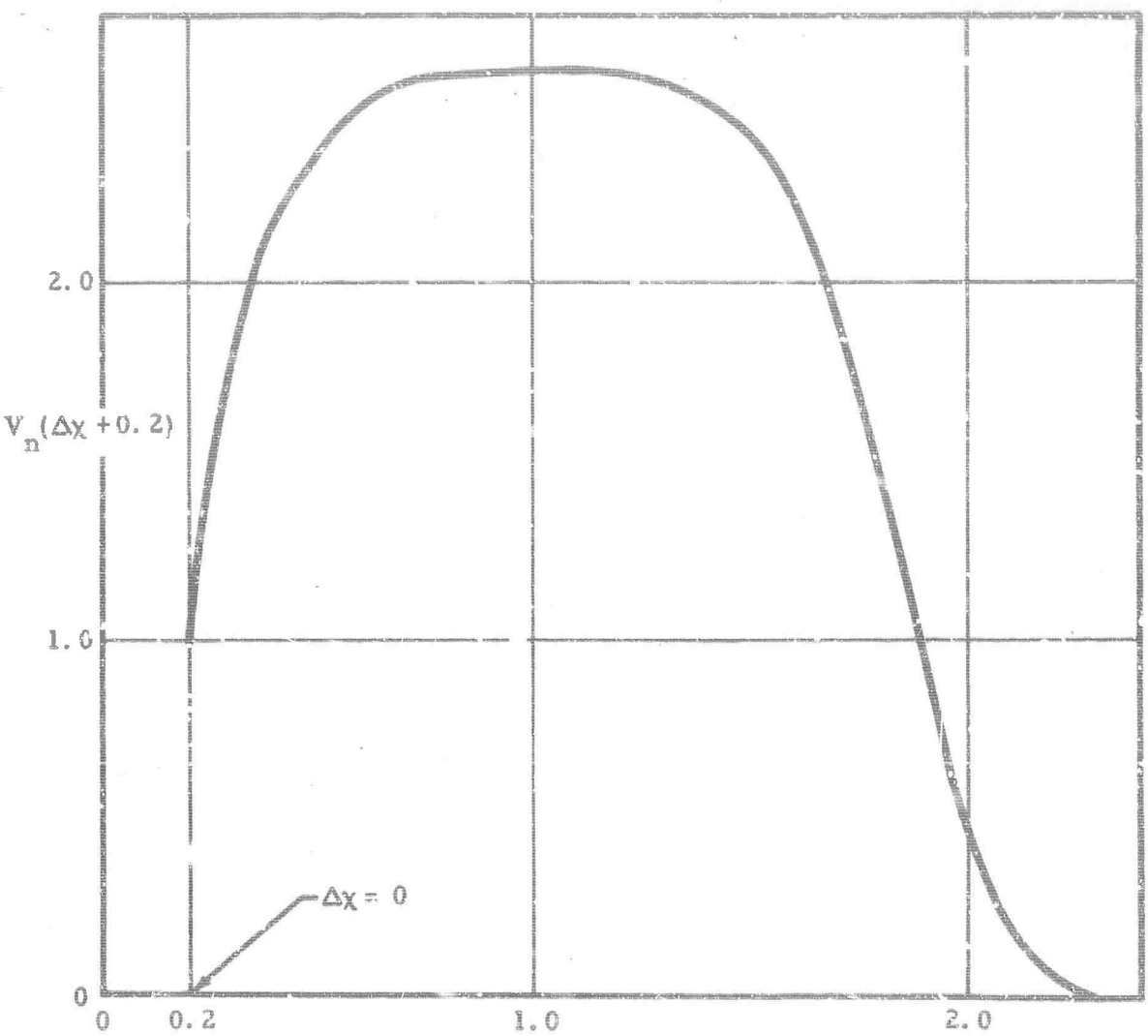

FIGURE 3.3
Normalized Light Transmission Curve of Optical System

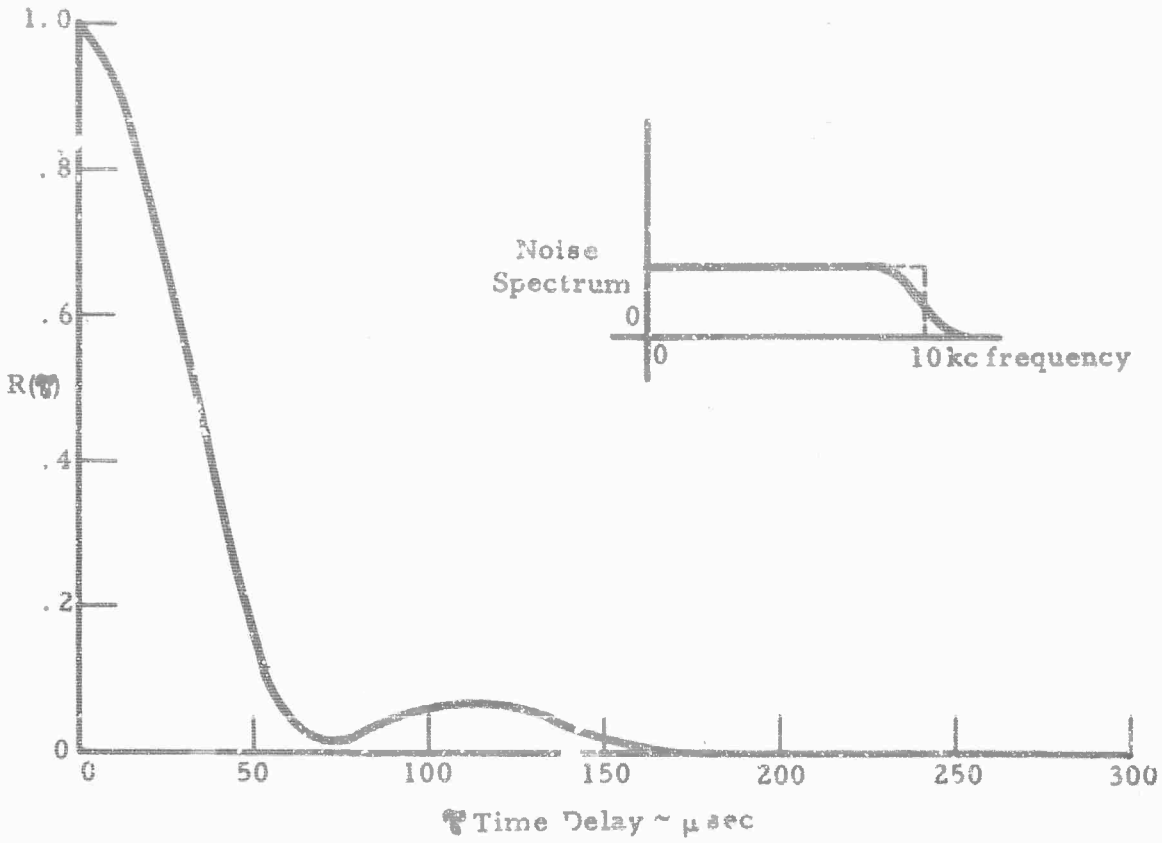

FIGURE 3.4
TEMPORAL CORRELATION OF WHITE NOISE

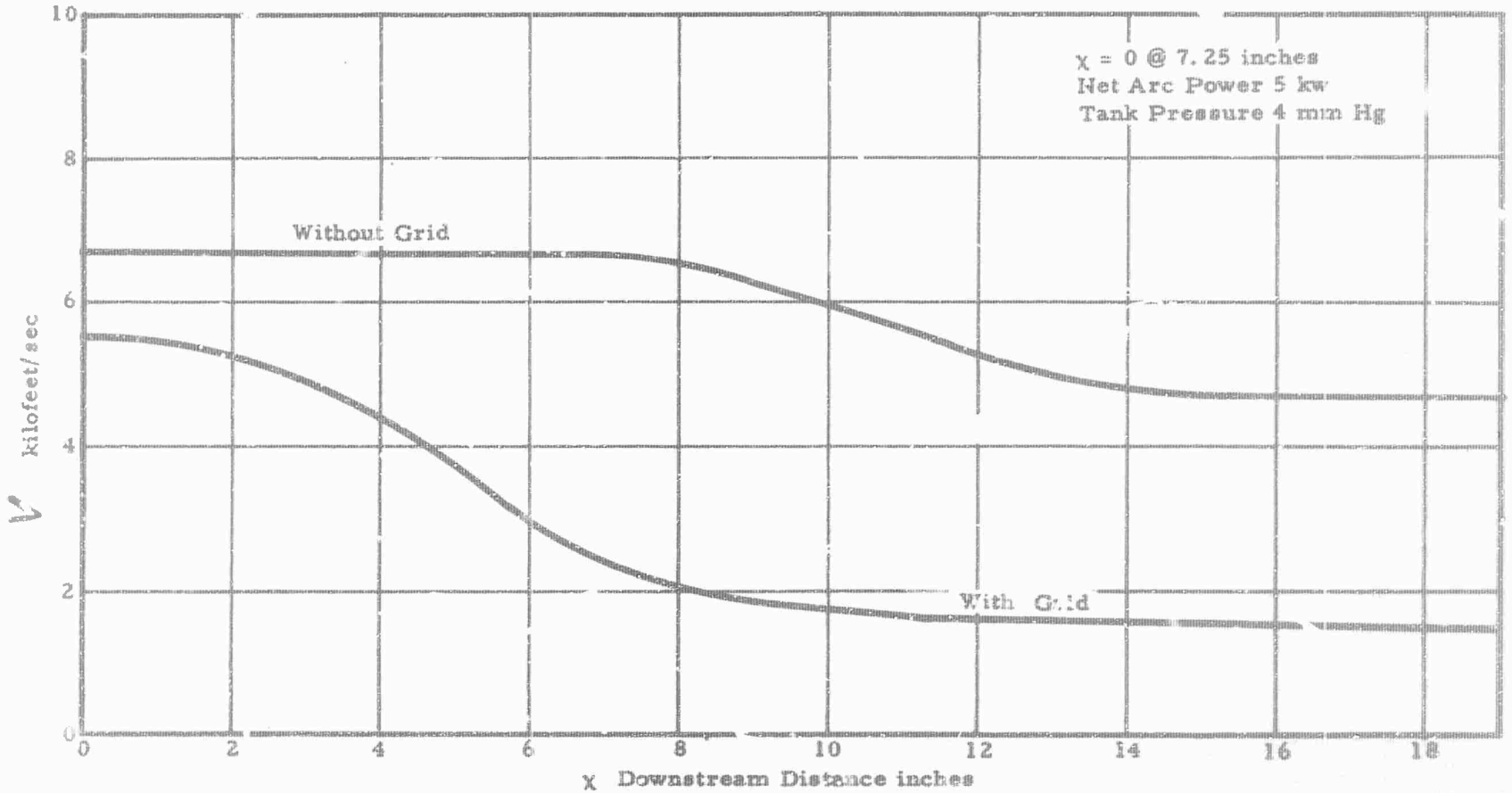

FIGURE 3.5

JET AXIAL VELOCITY vs AXIAL DISTANCE

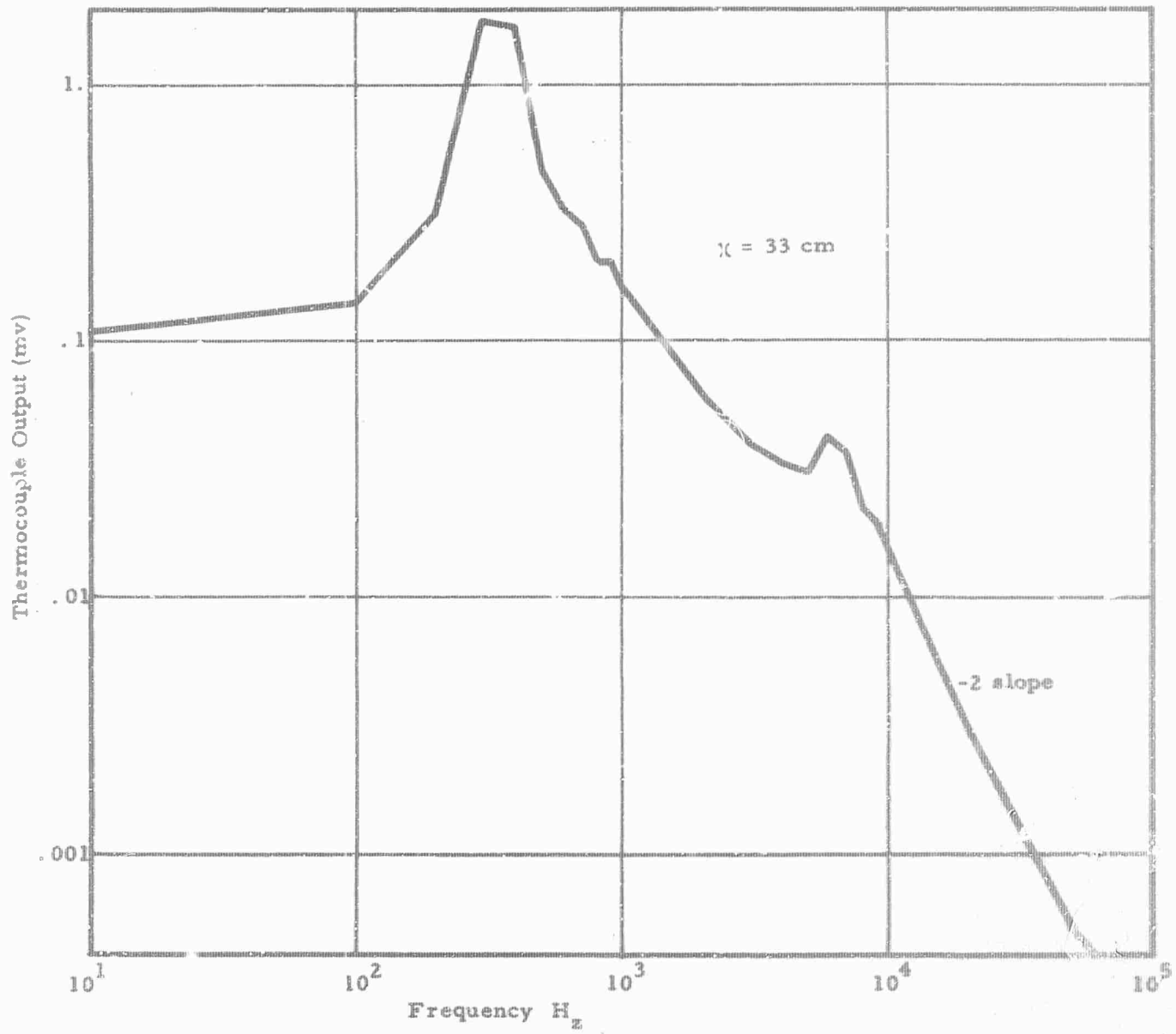

FIGURE 3.6
OPTICAL POWER SPECTRUM WITHOUT GRID

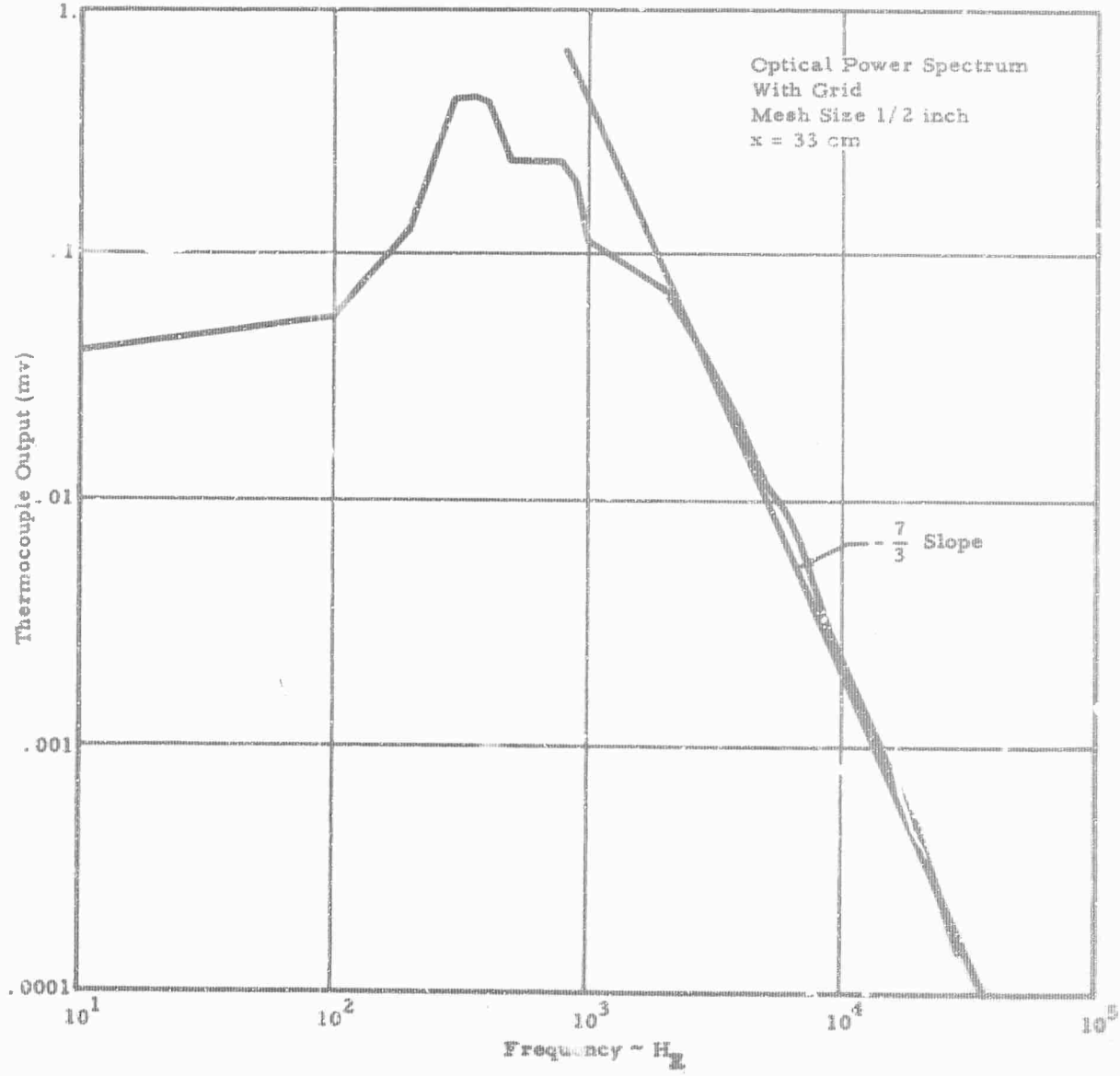
Optical Power Spectrum
With Grid
Mesh Size 1/2 inch
x = 33 cm
- 7/3 Slope
Thermocouple Output (mv)
1.
.1
.01
.001
.0001
10^1
10^2
10^3
10^4
10^5
Frequency ~ Hz

FIGURE 3.7

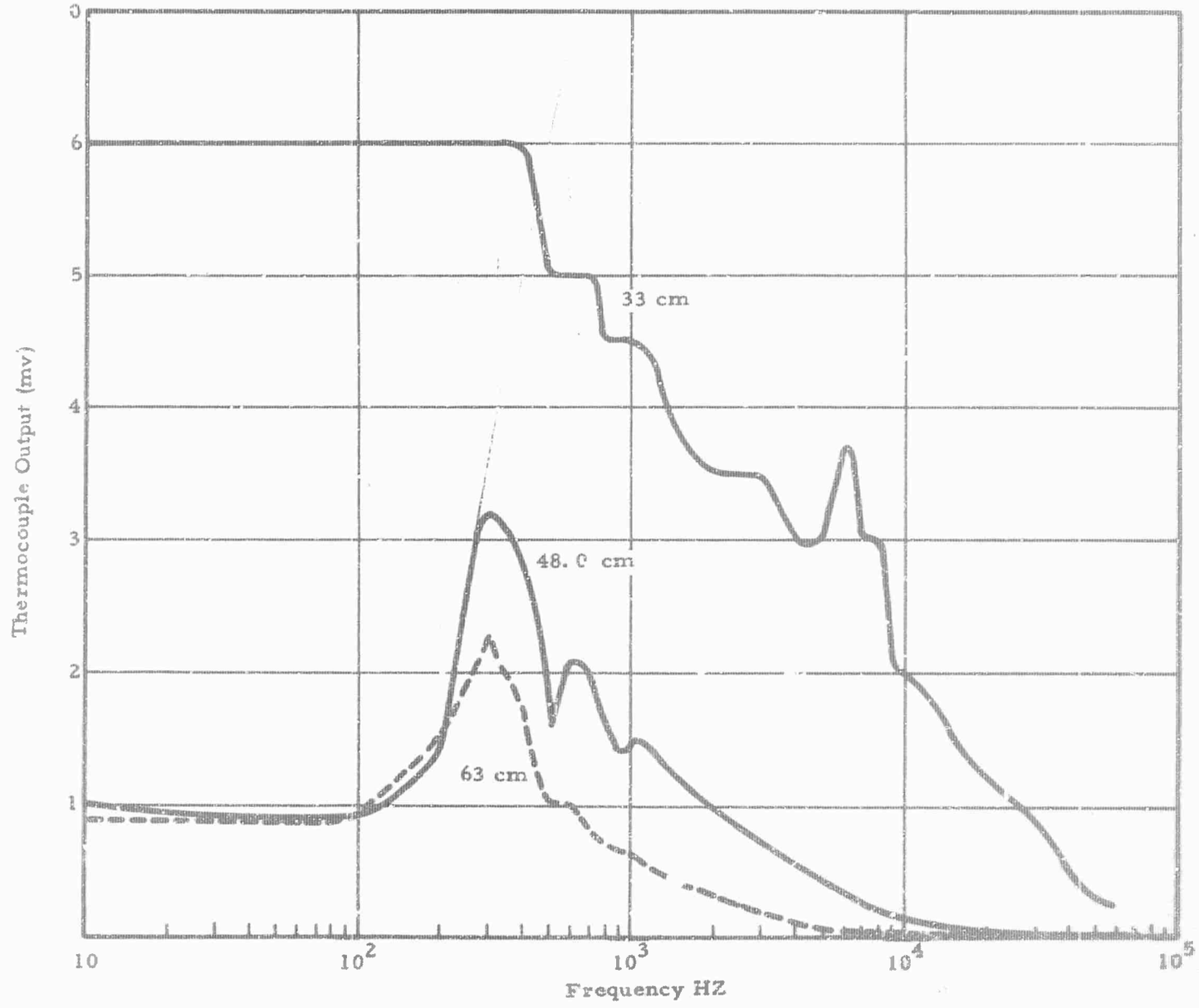

FIGURE 3.8
OPTICAL POWER SPECTRA vs DOWNSTREAM DISTANCE (No Grid)

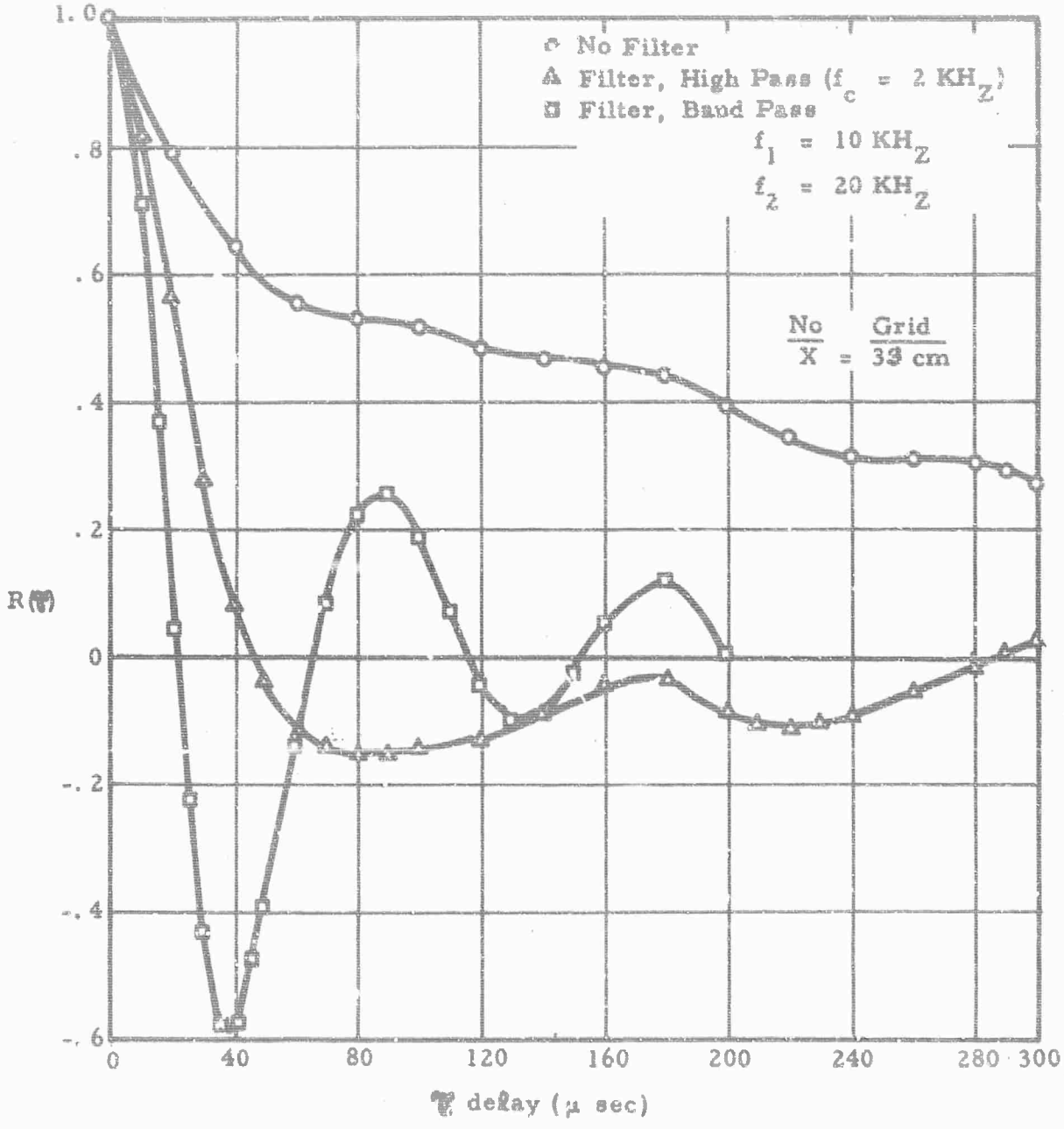

FIGURE 3.9

OPTICAL TEMPORAL CORRELATIONS

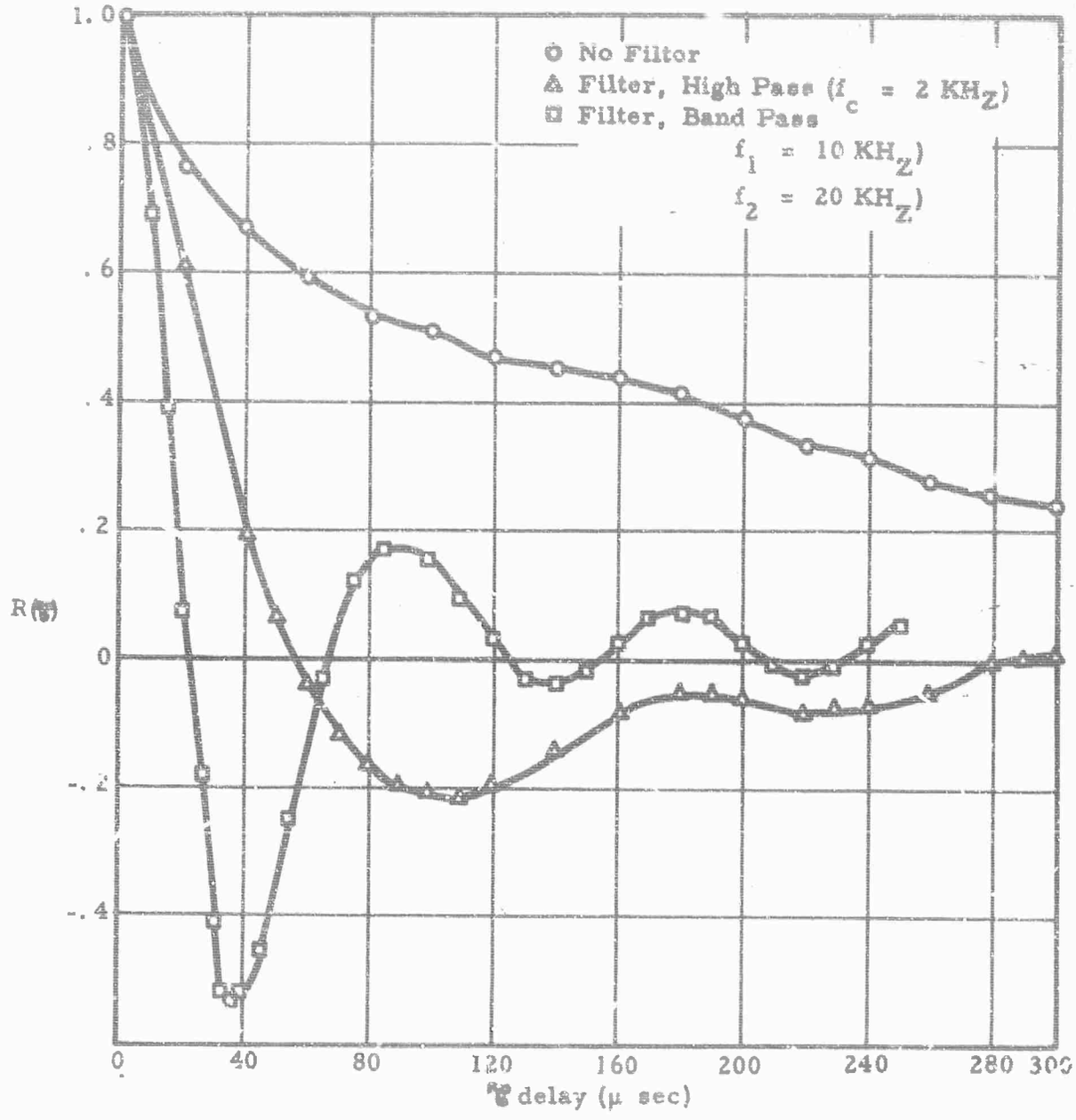

FIGURE 3.10

OPTICAL TEMPORAL CORRELATION WITH GRID (X = 33cm)

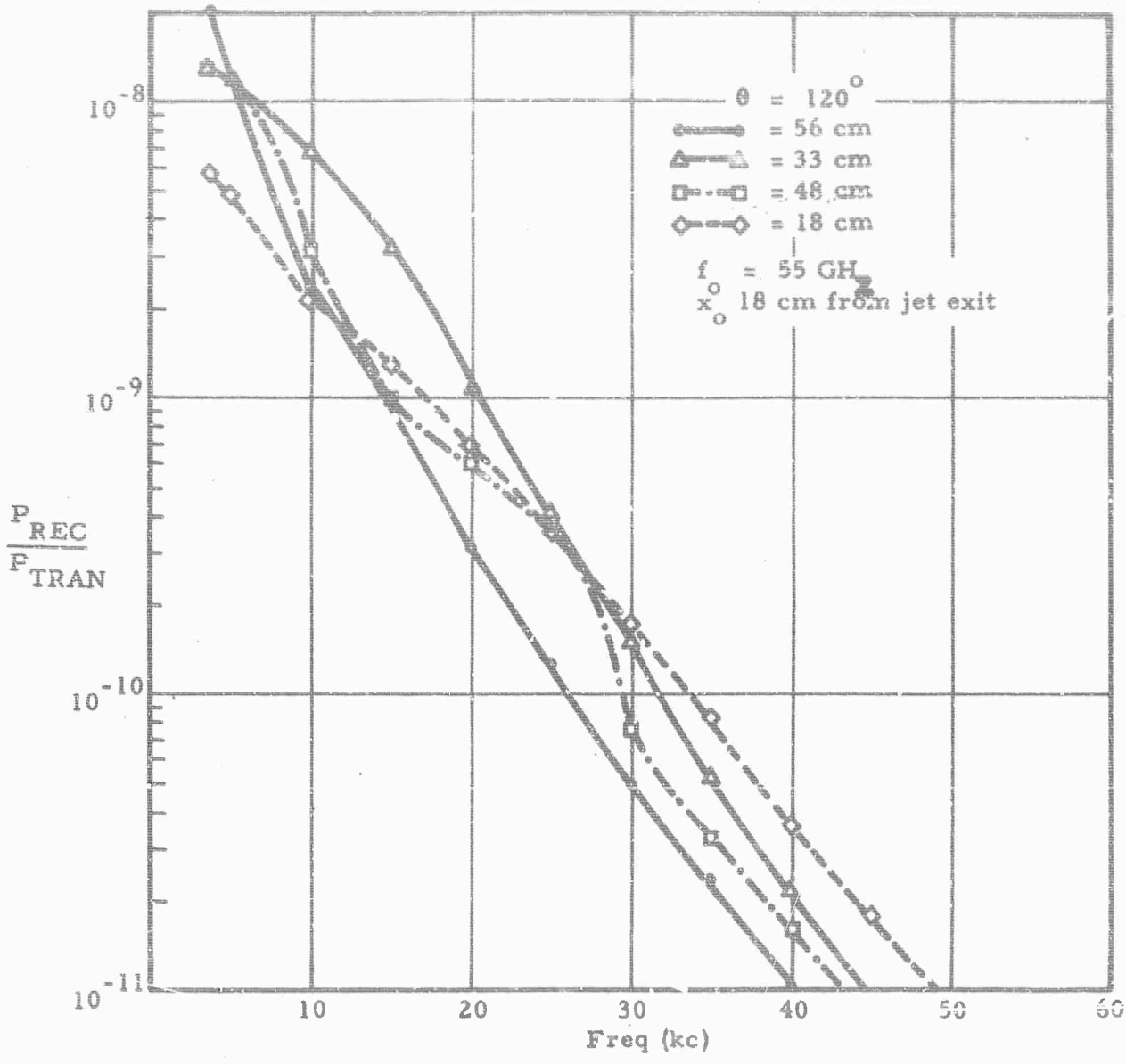

FIGURE 3.11

DOPPLER SPECTRA vs AXIAL DISTANCE

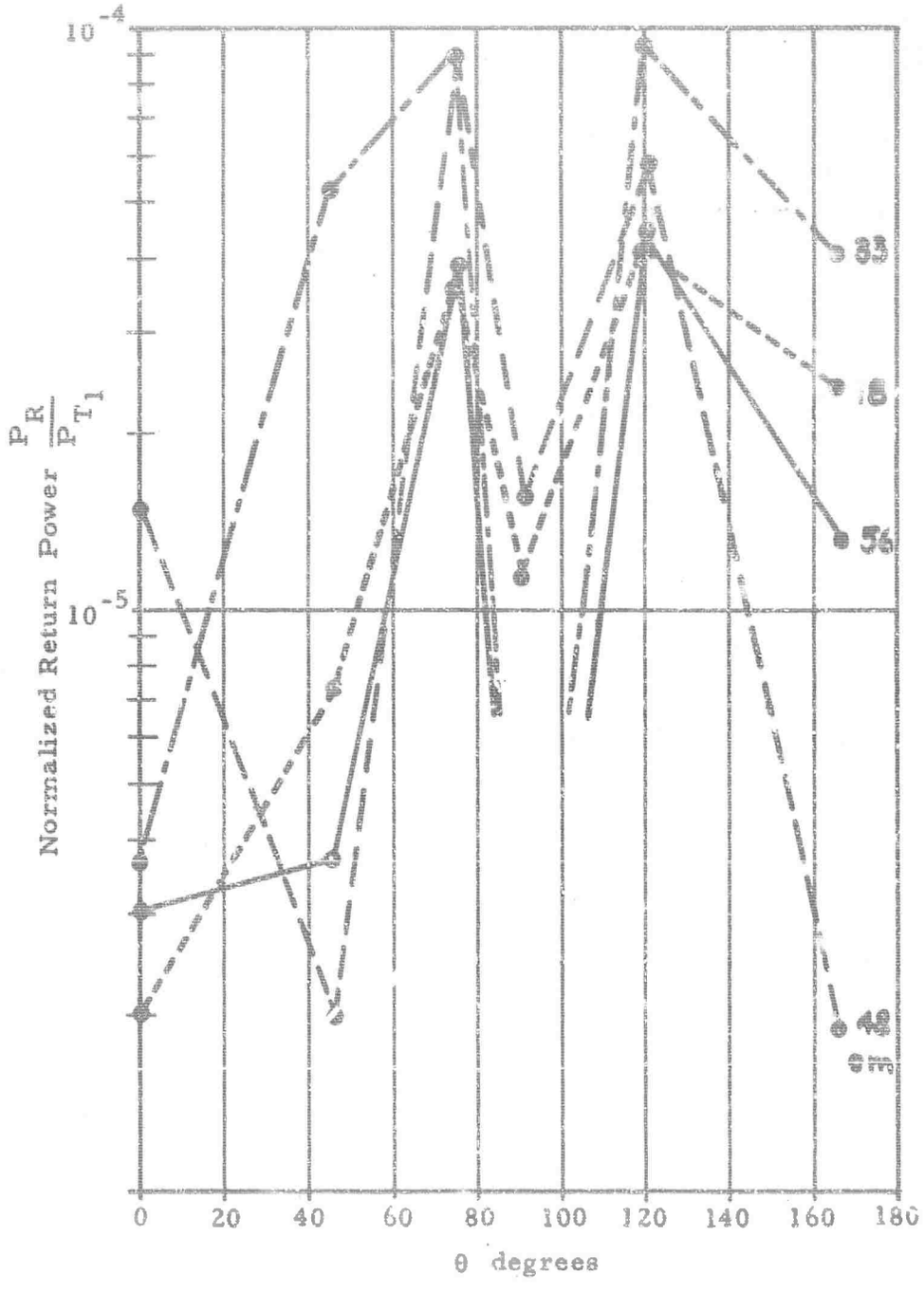

FIGURE 3.12
TOTAL DOPPLER RETURN POWER vs SCATTERING ANGLE - DISTANCE DOWNSTREAM A PARAMETER

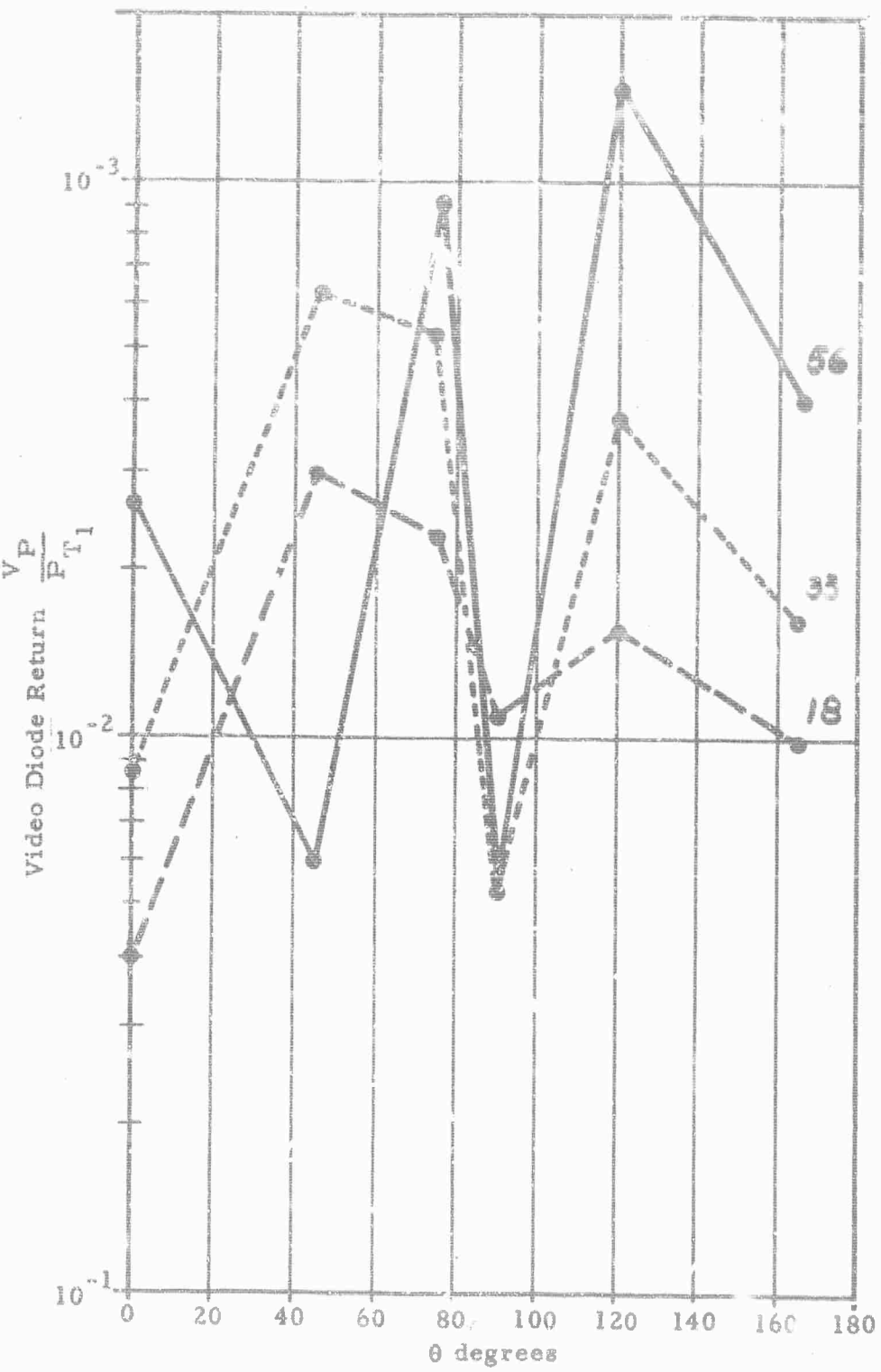

FIGURE 3.13

TOTAL RETURN POWER vs SCATTERING ANGLE - DOWNSTREAM DISTANCE A PARAMETER

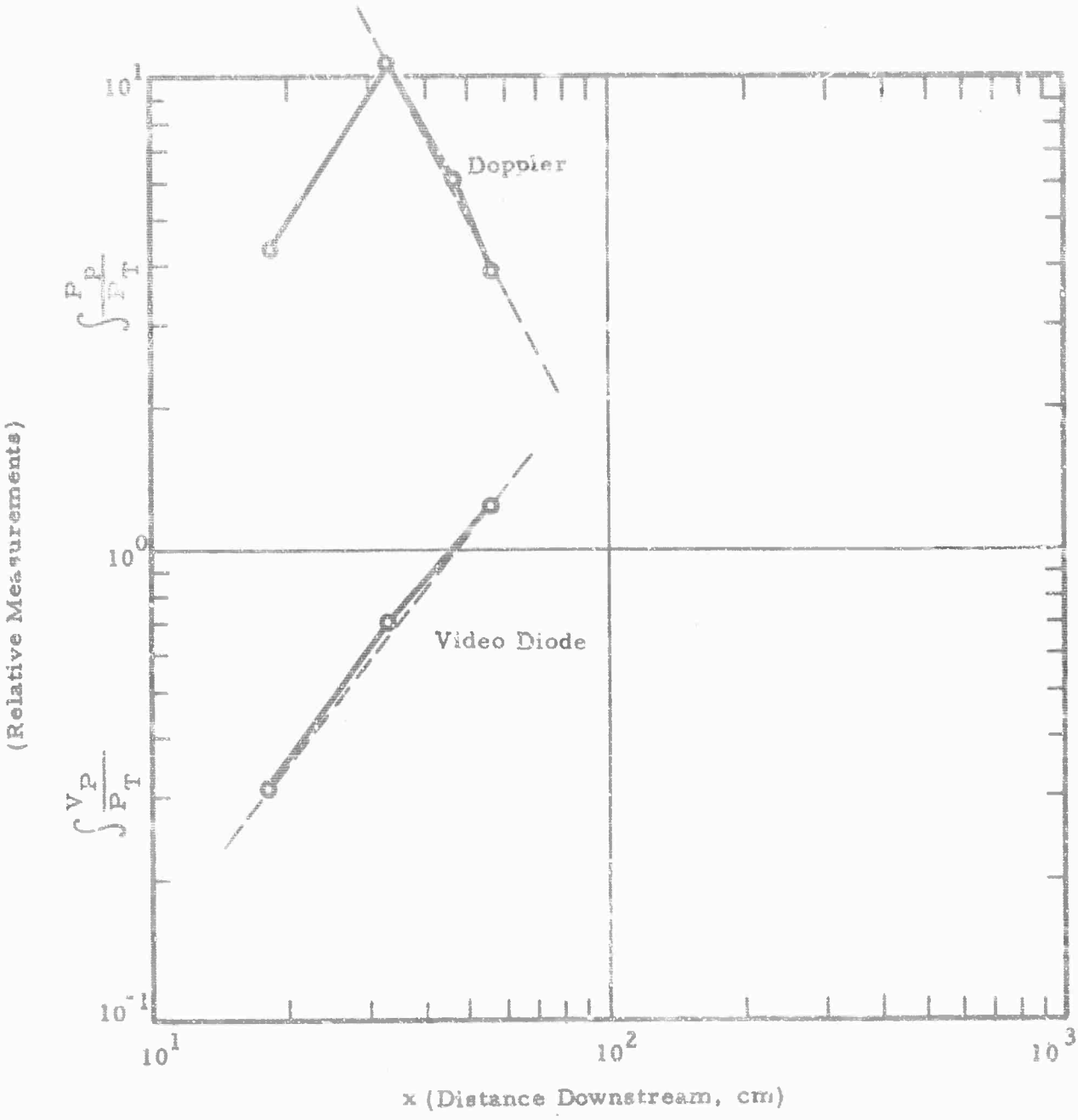

FIGURE 3.14

TOTAL SCATTERED POWER vs DOWNSTREAM DISTANCE

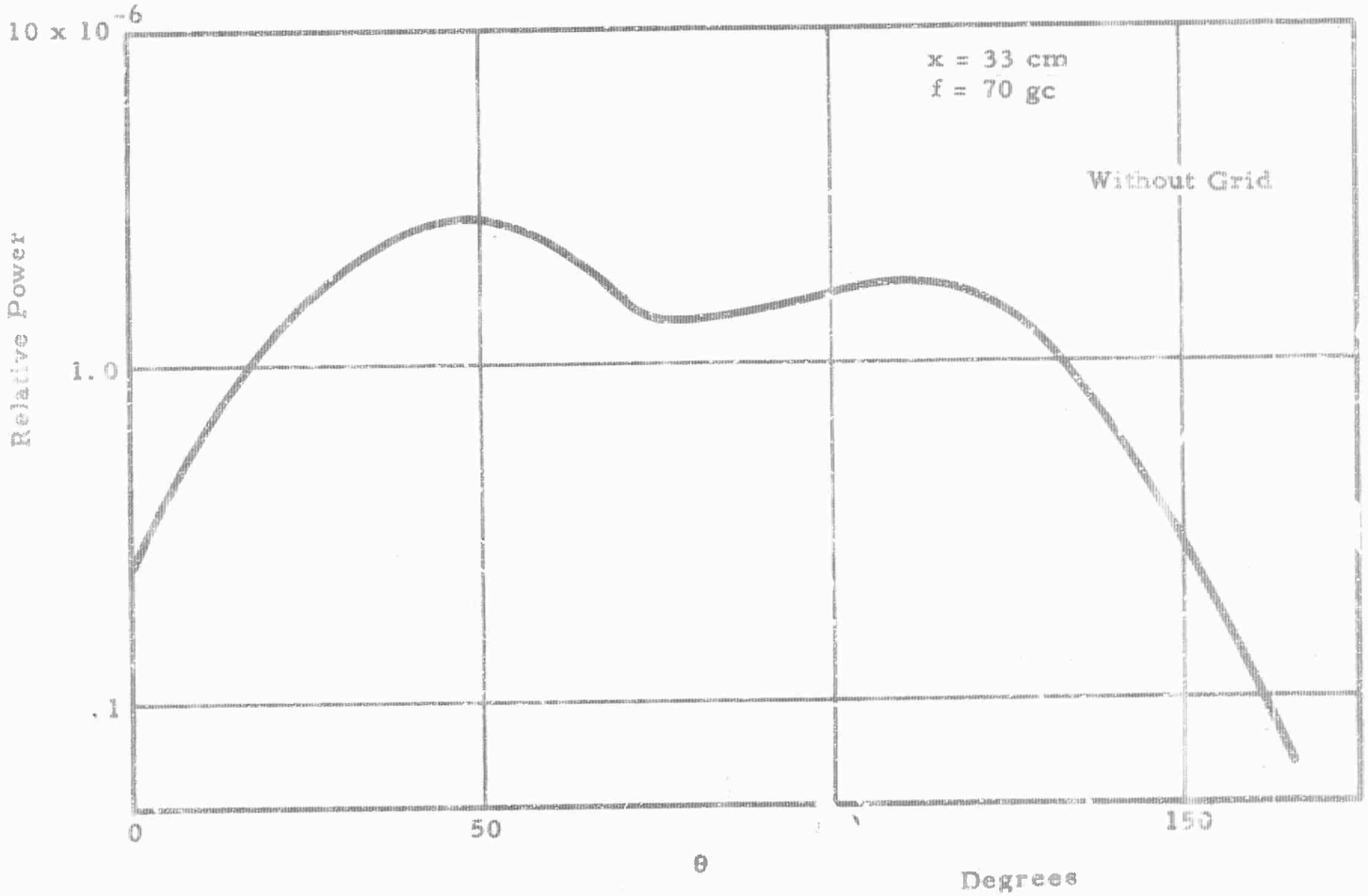

FIGURE 3.15

TOTAL DOPPLER RETURN POWER vs SCATTERING ANGLE
(f = 70 Gc)

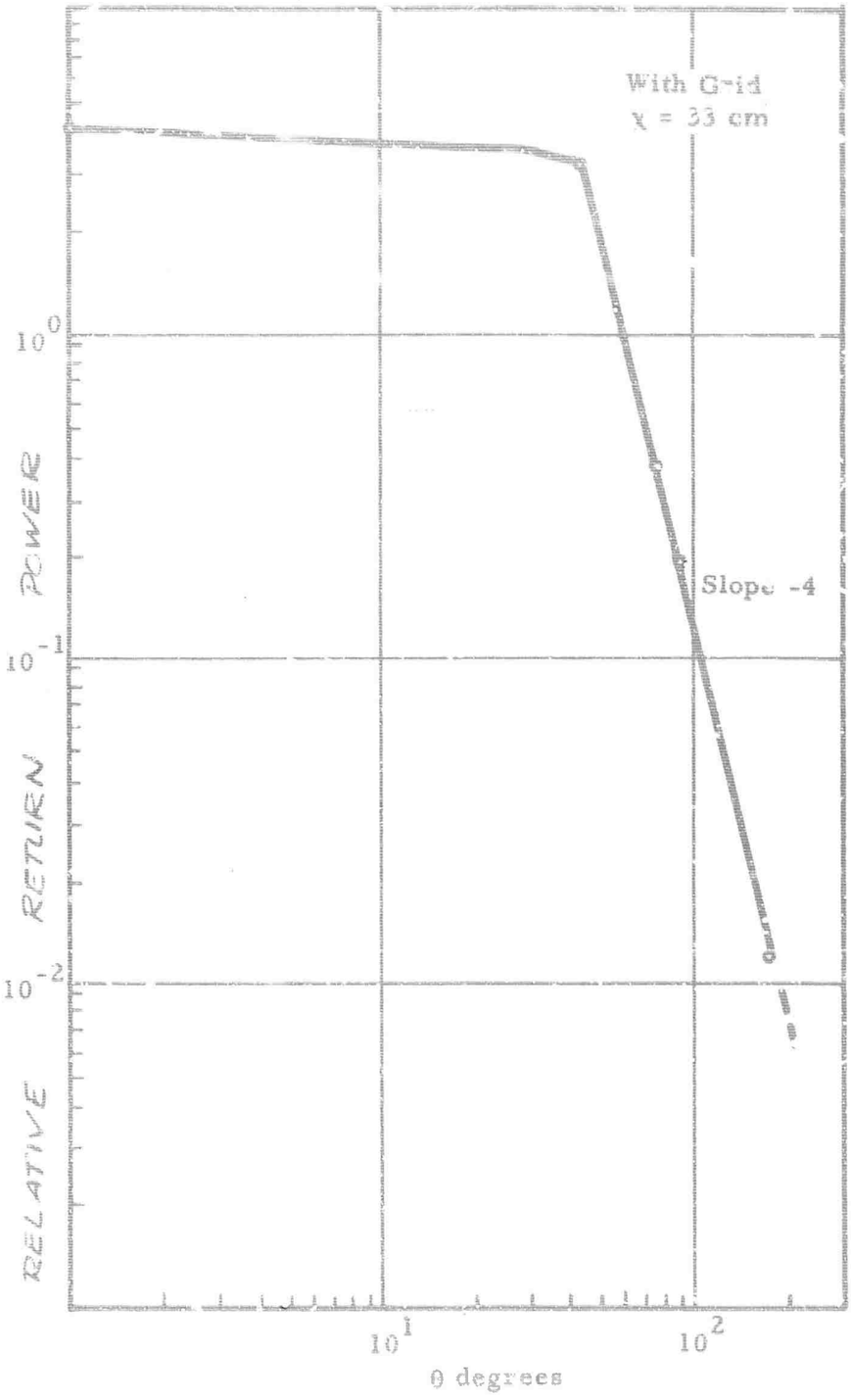

FIGURE 3.16
UNDERDENSE TOTAL DOPPLER SPECTRUM vs SCATTERING ANGLE

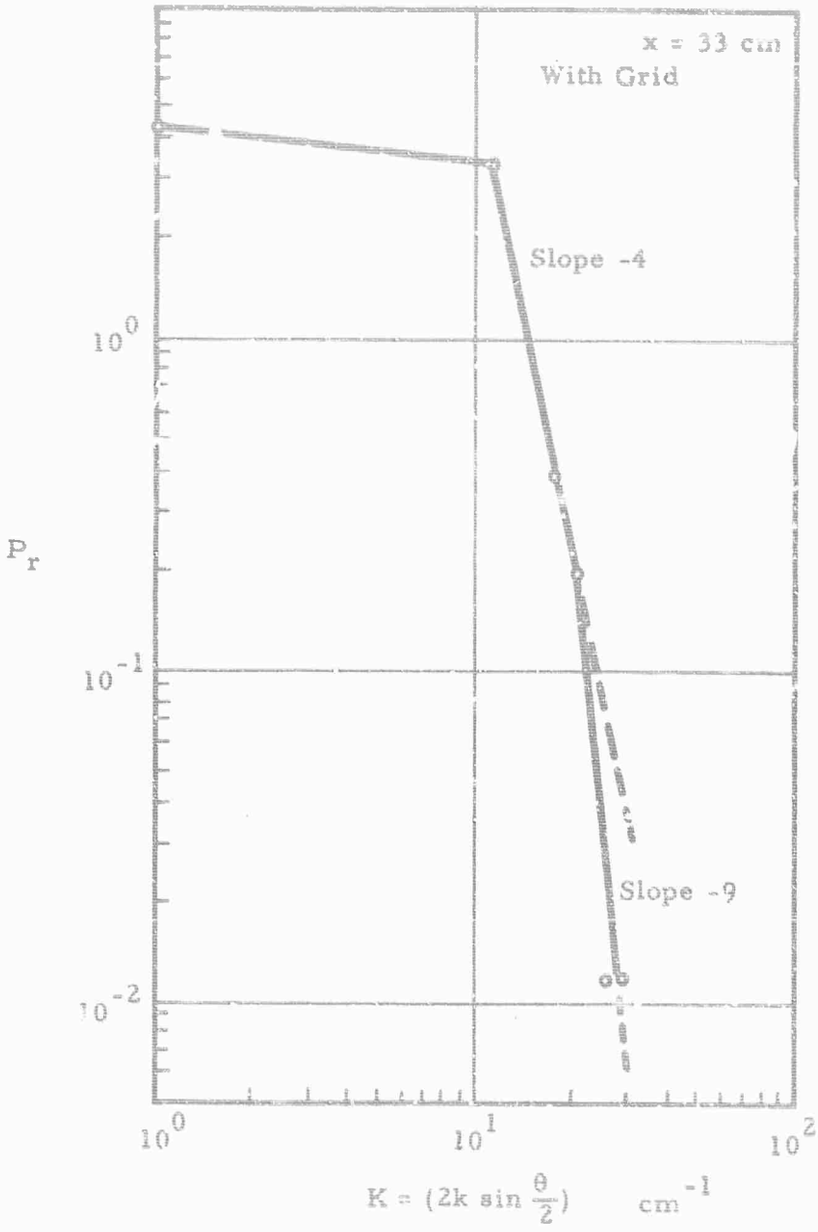

FIGURE 3.17
UNDERDENSE TOTAL DOPPLER POWER SPECTRUM vs TURBULENCE WAVE NUMBER
f = 70 Gc

SECTION 4

SUMMARY

Data on jet turbulence is being obtained steadily with the photo-spectro-correlator and the bistatic microwave probe. The two most interesting results have been the discovery of the null in the microwave signal scattered through 90° from an overdense plasma and the discovery that grid insertion demodulates the jet turbulence in a selective manner. The possibility of demodulating an RV'S oscillation superimposed on its wake is an interesting prospect.

The laser source for the shadowgraph system is expected in-house in January 1966. Its field of view (8") should be ideal in view of the photometric finding that the integral scale of the jet is of the order of 4 inches.

Gun development has progressed to the point where data rounds may soon be obtained using the instruments developed at CARDE. The necessity of enhancing the wake ionization to provide sufficient signal amplitude for some of the instruments is becoming apparent.

REFERENCES

1. R. D. Blackman and J. W. Tukey, The Measurement of Power Spectra, etc. Bell Systems Technical Journal, Volume 37, 1958.

2. Mario Cloutier, A Study of the CARDE 4 Inch Launcher Ballistic and Proofing, 9th ARA Meeting, Tullahoma, Tenn., October 18-20, 1965.

3. F. Motomura, Projectile Design Including Shock Phenomena in Models, 9th Aeroballistic Range Association Meeting, October 18-20, 1965.

4. C. Leech, Vibration Analysis, Aeroballistic Range Association Meeting, 18-20 October, 1965.